

ULTRASONIC SPRAY COATED INORGANIC THIN FILMS FOR
ELECTROCHROMIC APPLICATIONS

A THESIS SUBMITTED TO
THE GRADUATE SCHOOL OF NATURAL AND APPLIED SCIENCES
OF
MIDDLE EAST TECHNICAL UNIVERSITY



BY

ONUR TÜREL

IN PARTIAL FULFILLMENT OF THE REQUIREMENTS
FOR
THE DEGREE OF MASTER OF SCIENCE
IN
METALLURGICAL AND MATERIALS ENGINEERING DEPARTMENT

SEPTEMBER, 2017



Approval of the thesis

**ULTRASONIC SPRAY COATED INORGANIC THIN FILMS FOR
ELECTROCHROMIC APPLICATIONS**

Submitted by **ONUR TÜREL** in partial fulfillment of the requirements for the degree of **Master of Science in Metallurgical and Materials Engineering Department, Middle East Technical University** by,

Prof. Dr. Gülbin Dural Ünver _____
Dean, Graduate School of **Natural and Applied Sciences, METU**

Prof. Dr. Hakan Gür _____
Head of Department, **Metallurgical and Materials Eng. Dept., METU**

Assoc. Prof. Dr. Hüsnü Emrah Ünal _____
Supervisor, **Metallurgical and Materials Eng. Dept., METU**

Examining Committee Members:

Prof. Dr. Raşit Turan _____
Physics Dept., METU

Assoc. Prof. Dr. Hüsnü Emrah Ünal _____
Metallurgical and Materials Engineering Dept., METU

Assoc. Prof. Dr. Jongee Park _____
Metallurgical and Materials Engineering Dept., Atılım University

Assist. Prof. Dr. Mert Efe _____
Metallurgical and Materials Engineering Dept., METU

Assist. Prof. Dr. Görkem Günbaş _____
Chemistry Dept., METU

Date: 05.09.2017



I hereby declare that all information in this document has been obtained and presented in accordance with academic rules and ethical conduct. I also declare that, as required by these rules and conduct, I have fully cited and referenced all material and results that are not original to this work.

Name, Last name: Onur Türel

Signature :

ABSTRACT

ULTRASONIC SPRAY COATED INORGANIC THIN FILMS FOR ELECTROCHROMIC APPLICATIONS

Türel, Onur

MSc., Metallurgical and Materials Engineering Department

Supervisor: Assoc. Prof. Dr. Hüsnü Emrah Ünalın

September 2017, 61 pages

Recently, thin film transition metal oxides have been an important topic of optoelectronic device research due to high performance and low cost. Active layers in chromic devices and sensors, charge injection/transport layers of optoelectronic devices are only a few examples where transition metal oxide thin films are utilized. Tungsten oxide (WO_3), molybdenum oxide (MoO_3), titanium oxide (TiO_2) and vanadium oxide (V_2O_5) are the most frequently investigated thin film chemistries. Deposition of these materials in thin film form using different methods enables researchers to explore their properties and improve their performance.

Vacuum and solution based methods are two main deposition routes for thin films. In general, vacuum processes offer high homogeneity and purity, while solution based methods are less costly and practical. Comparison of device performances fabricated by these two branches yield critical data for the opportunity cost analysis.

Electrochromic devices have been a focus of research lately and they extensively utilize thin film transition metal oxides and conducting polymers. Transition metal oxides offer lower performance but higher stability compared to conducting

polymers. In addition, they adhere to the transparent conductive layer well and are highly compatible with common electrolytes.

In this work, the effect of thin film deposition route on the morphology and performance of MoO₃ based electrochromic (EC) devices was investigated. For deposition, ultrasonic spray pyrolysis (USP), thermal evaporation and sequential deposition (SD) of these two methods were used. MoO₃ thin films were then characterized using X-ray diffraction (XRD), X-ray photoelectron spectroscopy (XPS), scanning electron microscopy (SEM) and atomic force microscopy (AFM). Surface characteristics and chemical structure of the deposited thin films were found to depend extensively on the deposition route. EC performance and reversibility of the samples were evaluated using spectroelectrochemical methods and cyclic voltammetry. Sample prepared by USP method showed low coloration efficiency (CE) (16 cm² C⁻¹), but high stability. In contrast, sample prepared by thermal evaporation had high CE (30 cm² C⁻¹), but low stability. Sample prepared by SD method showed the highest CE (33 cm² C⁻¹) among other samples and maintained its stability with cycling. All in all, the SD route investigated in this work was found to be highly promising and can be simply extended to other metal oxide systems.

Keywords: Ultrasonic spray pyrolysis, thermal evaporation, sequential deposition, molybdenum oxide (MoO₃), electrochromics.

ÖZ

ELEKTROKROMİK UYGULAMA İÇİN ULTRASONİK SPREY KAPLANMIŞ İNORGANİK İNCE FİLMLER

Türel, Onur

Yüksek Lisans, Metalurji ve Malzeme Mühendisliği Bölümü

Tez Yöneticisi: Doç. Dr. Hüsnü Emrah Ünalın

Eylül 2017, 61 sayfa

Son zamanlarda yüksek performans ve düşük maliyetleri sebebiyle geçiş metal oksitlerinin ince filmleri optoelektronik cihaz arařtırmalarında önemli bir yer edinmiştir. Kromik cihazların ve sensörlerin aktif malzemeleri, optoelektronik cihazlardaki yük enjeksiyon ve taşıma tabakaları geçiş metali oksitlerinin kullanım alanlarından sadece birkaçıdır. Tungsten oksit (WO_3), molibden oksit (MoO_3), titanium oksit (TiO_2) ve vanadium oksit (V_2O_5) metal oksitler arasında en çok çalışılanlardır. Bu malzemelerin ince film şeklinde üretilmesine olanak sağlayan kaplama yöntemleri sayesinde arařtırmacılar filmlerin özelliklerini kolaylıkla inceleyebilmekte ve performanslarını iyileştirebilmektedir.

İnce filmler, vakum ve çözelti esaslı yöntemlerle kaplanmaktadır. Vakum esaslı yöntemler yüksek homojenlik ve saflık sağlarken, çözelti temelli yöntemler daha pratik ve düşük maliyetlidir. Bu iki yöntemle üretilen cihazların performanslarının karşılaştırılması fırsat maliyeti analizi için çok önemli veriler sağlamaktadır.

Elektrokromik cihazlar son yıllarda arařtırmacıların yoğun ilgisini çekmiştir ve bu amaçla genellikle ince film geçiş metal oksitleri ve iletken polimerler kullanılmaktadır. Geçiş metal oksitleri, iletken polimerlere göre daha düşük performans sunar ama daha yüksek dayanıma sahiptir. Ayrıca, saydam iletken katmana iyi yapışır ve yaygın olarak kullanılan elektrolitlerle uyumludurlar.

Bu çalışmada ince film kaplama yönteminin elektrokromik cihazlarda kullanılan MoO₃ ince filmlerin morfolojisi ve performansı üzerindeki etkisi incelenmiştir. Kaplama işlemi için ultrasonik spreycaplama (USP), termal buharlaştırma ve her iki yöntemin art arda kullanılması ilkesine dayanan ardışık kaplama yöntemleri kullanılmıştır. Kaplama sonrası MoO₃ ince filmler X-ışını kırınımı (XRD), X-ışını fotoelektron spektroskopisi (XPS), taramalı elektron mikroskobu (SEM) ve atomik kuvvet mikroskobu (AFM) ile karakterize edilmiştir. Kaplanan ince filmlerin yüzey özelliklerinin ve kimyasal özelliklerinin olarak kaplama yöntemine son derece bağlı olduğu gözlemlenmiştir. Numunelerin elektrokromik performansı spektroeletrokimyasal yöntem ve döngüsel voltametre ile değerlendirilmiştir. USP yöntemiyle hazırlanan numune renklenmede düşük verimlilik (16 cm² C⁻¹) ancak yüksek dayanım göstermiştir. Buna karşılık, termal buharlaştırma yöntemiyle hazırlanan numunelerin renklenme verimliliği (30 cm² C⁻¹) yüksek ancak dayanımı düşüktür. Ardışık kaplama yöntemiyle hazırlanan numune diğer numunelere göre renklenmede en yüksek verimliliği (33 cm² C⁻¹) göstermiştir ve döngüsel olarak da kararlıdır. Sonuç olarak, bu çalışmada elde edilen sonuçlar ardışık kaplama yönteminin gelecek vadettiğini ve diğer metal oksit sistemlerinde de kolaylıkla kullanılabileceğini göstermiştir.

Anahtar Kelimeler: Ultrasonik spreycaplama, termal buharlaştırma, ardışık kaplama, molibden oksit (MoO₃, elektrokromizm).



“No man ever steps in the same river twice, for it's not the same river and he's not the same man.”

Heraclitus

To Gülce, my family and my dear friends,

ACKNOWLEDGEMENTS

This work was supported by The Scientific and Technological Research Council of Turkey (TÜBİTAK) via, “Priority Fields Support Program (2210-C)”.

Firstly, I would like to express my deepest gratitude to my advisor Assoc. Prof. Dr. H. Emrah Ünalın, for his support, guidance and patience throughout the study. It is a great honor to work under his supervision.

I owe my deepest gratitude to my labmates and dearest friends, Şahin Coşkun, Recep Yüksel, Doğa Doğanay, Alptekin Aydınlı, Mete Batuhan Durukan, Selin Özkul, Sevim Polat, Ece Alpugan, İtır Bakış Doğru, İpek Bayraktar, Serkan Koylan, and Şeyma Koç.

I also appreciate the great moral support from my dearest friends; Meriç Akyıldız, Aydın Bozkuş, Toygun Çetinkaya, Deniz Boztemur, Çağan Elbistanlıođlu, İsmet Gökhan, Mert Kılıç, Ozan Öztürk, İmre Özbay, Özgün Sönmez, Dođancan Tigan, Deniz Turan, Kerem Tuncel and Mert Volkan.

Finally, I must express my very profound gratitude to my parents and Gülce for providing me with unfailing support and continuous encouragement throughout my years of study and through the process of researching and writing this thesis. This accomplishment would not have been possible without them. Thank you.

TABLE OF CONTENTS

ABSTRACT.....	v
ÖZ.....	vii
ACKNOWLEDGEMENTS	x
LIST OF FIGURES.....	xiii
LIST OF TABLES.....	xv
CHAPTERS	
1. INTRODUCTION	1
1.1. Thin Film Deposition Methods	1
1.1.1. Physical Vapor Deposition (PVD).....	3
1.1.1.1. Thermal Evaporation	3
1.1.1.2. Sputter deposition	4
1.1.1.3. Ion Plating.....	4
1.1.2. Chemical Vapor Deposition (CVD)	5
1.1.2.1. Plasma Enhanced Chemical Vapor Deposition (PECVD).....	6
1.1.2.2 Atomic Layer Deposition (ALD).....	6
1.1.3. Sol-Gel Methods.....	7
1.1.3.1. Spray Pyrolysis	7
1.2. Transition Metal Oxides.....	10
1.2.1. Molybdenum Oxide (MoO_3)	10
1.2.2. Tungsten Oxide (WO_3).....	13
1.2.3. Titanium Oxide (TiO_2)	13
1.3. Electrochromic (EC) Devices.....	14
2. EXPERIMENTAL DETAILS	23

2.1. Ultrasonic Spray Pyrolysis (USP) System	23
2.2. Deposition by USP	24
2.3. Deposition by Thermal Evaporation	25
2.4. Sample Preparation.....	26
2.5. Characterization and EC Characteristics	27
3. RESULTS AND DISCUSSION	29
3.1. Optimization of USP method	29
3.2. Characterization.....	31
3.2.1. XRD Measurements	31
3.2.2. XPS Measurements.....	32
3.2.3. SEM Imaging.....	36
3.2.4. AFM Imaging and Measurements.....	37
3.3. EC Performance.....	39
3.4. Effect of SD Technique	49
4. CONCLUSIONS AND FUTURE WORK	51
REFERENCES.....	53
CURRICULUM VITAE	61

LIST OF FIGURES

Figure 1.1 Thin film deposition methods.....	2
Figure 1.2 Schematic representation of the physical deposition methods, a) thermal evaporation, b) sputter deposition and c) ion plating.....	5
Figure 1.3 Schematic representation of the spray pyrolysis equipment.....	8
Figure 1.4 Crystal structure of orthorhombic α -MoO ₃	11
Figure 1.5 Electrophosphorescence spectra of SOLED configurations [26].	12
Figure 1.6 Elements of the periodic table with electrochromic oxides. Type of electrochromism is provided in the legend [86].....	14
Figure 1.7 A full cell electrochromic device based on WO ₃ and ITO [85].	15
Figure 1.8 SEM images of the (a) as deposited and (b) annealed (450°C) films prepared by electrodeposition. [87].....	17
Figure 1.9 SEM images of the MoO ₃ thin films annealed at (a) 100, (b) 200, (c) 300, (d) 350, (e) 400 and (f) 500°C [28].	18
Figure 1.10 Top-view (i) and cross-sectional (ii) SEM images of the (a) bare Nb ₂ O ₅ and MoO ₃ , (b) 40 cycles and (c) 120 cycles [88].....	21
Figure 1.11 Kinetic transmittance change of the samples at the applied voltages from ± 0.25 to 1.00 V [88].	22
Figure 2.1 Photograph of the home made USP system.....	24
Figure 2.2 Precursor solutions prepared by dissolving MoCl ₅ in UP water. Molarities of the solutions from left to right are 1, 5 and 10 mM respectively.....	25
Figure 2.3 A photo showing various samples deposited by USP method on ITO coated glass substrates.....	27
Figure 3.1 Effect of USP parameters on the end product and SEM images collected from such cases.	31
.....	32
Figure 3.2 X-ray diffraction pattern of the samples (JCPDS card No: 05-0508).	32
Figure 3.3 Survey spectra of SD-A sample.....	33
.....	35

Figure 3.4 High-resolution regional XPS spectra of the samples corresponding to (a) Mo 3d 3/2 and Mo 3d 5/2 and (b) O 1s for the samples.	35
Figure 3.5 Top-view SEM images of (a) PVD, (b) PVD-A, (c) USP-A and (d) SD-A samples. All scales are the same.	37
Figure 3.6 Topographical AFM 3D and 2D images of the USP-A (a,b), PVD-A (c,d) and SD-A (e,f) samples.	38
Figure 3.7 CV results of the samples (a) USP-A, (b) PVD-A and (c) SD-A.	41
Figure 3.8 Transmittance plots for (a) USP-A, (b) PVD-A and (c) SD-A samples in bleached and colored states.	43
Figure 3.9 Electrochromic repeated switching and optical transmittance change and applied current with respect to time graphs of (a,d) USP-A, (b,e) PVD-A and (c,f) SD-A sample monitored at 700 nm.	45

LIST OF TABLES

Table 1.1 Parameters and their origins of the USP system.....	9
Table 1.2 EC performance of the MoO ₃ thin films at different annealing temperatures [28].....	19
Table 2.1 Designations and descriptions of the samples.....	27
Table 3.1 AFM results of USP-A, PVD-A and SD-A thin films of samples. Ra (average roughness) and RMS (root mean square roughness) values of each film are given.....	39
Table 3.2 Switching time of the samples for 10 % transmittance change.....	46
Table 3.3 Injected charge, transmittance values of bleached and colored states, OD and CE of the samples at initial and 20th cycle.....	48



CHAPTER 1

INTRODUCTION

1.1. Thin Film Deposition Methods

Today, computers, micro and some of macro electronic equipment rely on thin film technology. The industry of such devices created a major demand on thin film technology for the improved quality and fabrication control to produce sophisticated electronic devices. By the successful research conducted on thin film (thickness $< 1 \mu\text{m}$) deposition, improved quality and economical ways for the deposition was found. Another aspect that made such advancement possible was the progression on physics, chemistry, and other fundamental sciences that improved the understanding on the mechanism of thin films [1].

Thin film deposition technique has a great influence on the performance of the final product. Even though the thin films are deposited using the same method, the differences in crystal structure, microstructure and impurities result in thin films with different properties. Surface area and porosity are some other key factors that affect the device performance. Historical thick coating methods enable too less control over the final product. Research in this field deliver practical and cost efficient alternative methods that allow extensive control over the deposited film structure, which also enables development of various devices. Progress in thin film research is therefore a building block for the optoelectronic devices.

In principle, thin film deposition methods can be divided into two main groups. These are chemical and physical methods. Chemical methods involve electroplating, sol-gel and chemical vapor deposition methods, while physical methods consist of thermal evaporation, sputter deposition and ion plating. A graph showing this classification is provided in Figure 1.1.

THIN FILM

CHEMICAL METHODS

❑ ELECTROPLATING

❑ SOL-GEL

- SPRAY PYROLYSIS
- SPIN COATING
- DIP COATING

❑ CHEMICAL VAPOR DEPOSITION

- MOCVD
- PECVD
- ATOMIC LAYER DEPOSITION

PHYSICAL METHODS

❑ PHYSICAL VAPOR DEPOSITION

- THERMAL EVAPORATION
- ION PLATING
- LASER ABLATION
- MOLECULAR BEAM EPITAXY
- ELECTRON BEAM

❑ SPUTTER DEPOSITION

- RF
- DC
- MAGNETRON

Figure 1.1 Thin film deposition methods.

1.1.1. Physical Vapor Deposition (PVD)

Physical vapor deposition (PVD) processes involve atom by atom deposition to fabricate thin film layers. To conduct a PVD deposition, a material is evaporated from solid or in liquid form to transport its atoms or molecules to the substrate. Environment for PVD is either a vacuum or low pressure gaseous environment. The substrate used to deposit thin films can be in complex geometries and rate of deposition can be 10-100 Å/s.

Deposition of thin films, both as elements and alloys is possible through PVD processes. Deposition of a compound thin film can be carried out with co-deposition, which means evaporation of more than one materials simply through placing all into the evaporation source. Another route to follow for the deposition of a compound thin film is through the placement of deposited thin films under a reactive low pressure environment [2].

PVD can be categorized as thermal evaporation (vacuum deposition), sputter deposition, ion plating, laser ablation and molecular beam epitaxy. Schematic representation of the physical methods is given in Figure 1.2.

1.1.1.1. Thermal Evaporation

To conduct deposition via thermal evaporation, source material is placed into the pot (crucible) of the evaporator in a vacuum environment. Source material is then evaporated by the heat generated through a heating filament. Temperature of the pot must be high enough to conduct evaporation at the corresponding pressure. Pressure of the environment must be as low as 10^{-5} to 10^{-9} Torr to prevent collision of the evaporated molecules with the gas molecules in the chamber. A rotating substrate is generally used to improve the homogeneity of the deposited thin films.

1.1.1.2. Sputter deposition

Another physical thin film deposition route is sputter deposition. In this method, target material is not evaporated by the thermal effect. Unlike thermal evaporation, particles are ejected from the target physically by the help of highly energetic bombarding particles. With enough energy, molecules are transferred from the target to the substrate. The distance between the target and the substrate is lower than thermal evaporation method. Bombardment of ions onto the target can be performed by an ion gun, a generated low pressure or high pressure plasma. Similar to thermal evaporation method, compounds can be deposited by involving a reactive gas in the plasma environment. Depending on the type of the power supply, radio frequency (RF), direct current (DC) are the most frequently used sputtering types.

1.1.1.3. Ion Plating

In ion plating method, target material is subjected to high current flow and low voltage to evaporate particles. By this application, atoms with similar electric charges are ionized. Particles emitted from the target is then delivered to the substrate with the force produced by opposite charged electric voltage applied to the substrate. Resulting thin film strongly adheres to the substrate [3].

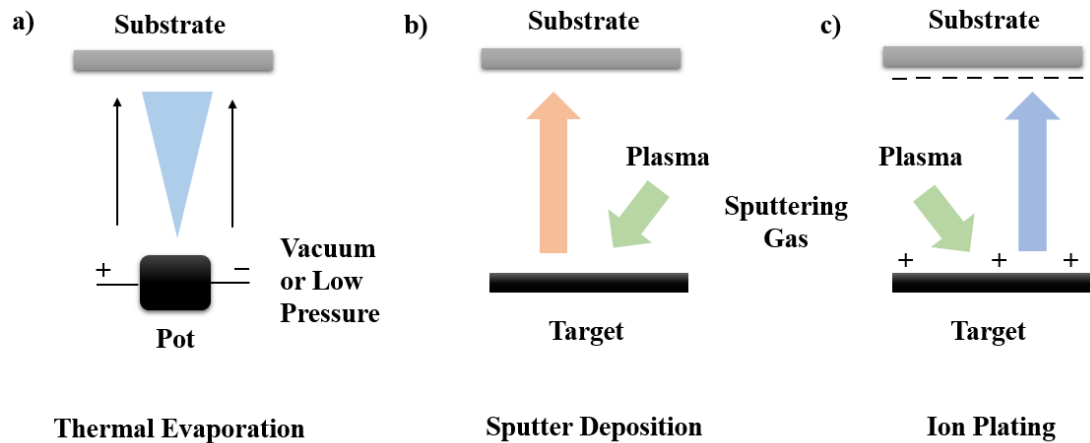


Figure 1.2 Schematic representation of the physical deposition methods, a) thermal evaporation, b) sputter deposition and c) ion plating.

1.1.2. Chemical Vapor Deposition (CVD)

Chemical vapor deposition (CVD) is a process that utilizes gas phase chemical reactions to form a solid material on a substrate. There are basically 4 processing steps; production of the required gas by heating the source, transportation of the gas to the substrate, deposition of the film by a chemical reaction as a result of adsorption of the gas and transportation of waste products away from the substrate. CVD is operated under vacuum and generally conducted at elevated temperatures. The main area of use is the application of solid thin-film coatings to surfaces. Wide range of materials could be deposited by CVD. They can be in the pure elemental form or in the product form, such as oxides and carbides. CVD has a lot of advantages in the use of deposition of thin film materials. Most importantly, CVD offers conformal deposition of thin films over a substrate. Since CVD utilizes chemical reactions, thickness of the film is independent from the surface geometry. Therefore, even complex shapes can be deposited homogeneously using this method. Moreover, since CVD is operated under vacuum materials can be deposited with very high purity. High deposition rates are possible due to its high temperature requirement. On the other hand, CVD has a number of disadvantages. The major disadvantage is the requirement of elevated temperatures. This restricts the kind of

substrates that can be used for the deposition. Besides that, complex processes used for the depositions may generate toxic and corrosive gases which are difficult to be removed [4]. To solve some of these problems and to enhance the performance of the deposition system, some special CVD methods are used, such as plasma enhanced chemical vapor deposition (PECVD) and atomic layer deposition (ALD).

1.1.2.1. Plasma Enhanced Chemical Vapor Deposition (PECVD)

PECVD is a type of CVD process in which thin film materials can be deposited onto a substrate at a lower temperature than standard CVD. In PECVD, parallel electrodes are placed around reactant gases. These electrodes excite the gases into plasma which trigger the chemical reaction. In this way, thin films can be deposited onto the substrates. The major advantage of PECVD over CVD is the reduction of the substrate temperature. In PECVD method, the substrate is commonly heated to 250 to 350°C, while in CVD it is generally heated above 1000 °C. Therefore, a wider range of substrate materials can be used for PECVD [5].

1.1.2.2 Atomic Layer Deposition (ALD)

ALD is a vapor phase technique which produces variety of thin film materials based on self-limiting, sequential reactions. In ALD, there are 2 precursors and both of them inserted as a series of sequential, non-overlapping pulses. Before inserting the other precursor, the one in use is purged from the chamber. Therefore, in each cycle only one monolayer of the material is deposited at the surface by the chemical reaction between these precursors. The process is cycled until the appropriate film thickness is obtained. The temperature requirement for ALD is modest that is lower than 350°C. The major advantage of ALD is the precise thickness control. The thickness of the film can be adjusted by utilizing layer-by-layer deposition [6].

1.1.3. Sol-Gel Methods

Sol gel methods involve formation of a substrate from a fluid solution. Process is carried out phenomenon such by draining, condensation and evaporation of the solvent. Mass production of thin film devices requires cost effective fabrication methods. Vacuum processes enable deposition of highly pure and homogeneous thin films [7]. However, it is time consuming and expensive. Ultrasonic spray pyrolysis (USP) is such a solution based alternative method for the deposition of metal oxide thin films [15–18]. This method involves a volatile precursor to be atomized by ultrasonication, followed by the deposition of the thin film onto a hot substrate [12]. Thermal evaporation, on the other hand, is a physical vapor deposition (PVD) process for the deposition of thin films. It is a vacuum based method and enables deposition of high quality films. During evaporation, the deposited material transforms physically, maintaining its chemical properties throughout the process [2].

1.1.3.1. Spray Pyrolysis

Spray pyrolysis is another thin film deposition method. It can be used for the production of dense and porous films, coatings and also powders [13, 14]. In addition to being a practical deposition method in terms of equipment and operation, it is also cost effective in terms of the used precursors. Precursors for the thin film deposition can be easily prepared through the dissolution of an appropriate salt in a common solvent. The deposition substrate can be chosen from a wide range of materials and deposition can performed over large areas using a moving stage. Deposition with such a system results in the deposition of highly homogeneous thin films. Schematic representation of the equipment is provided in Figure 1.3.

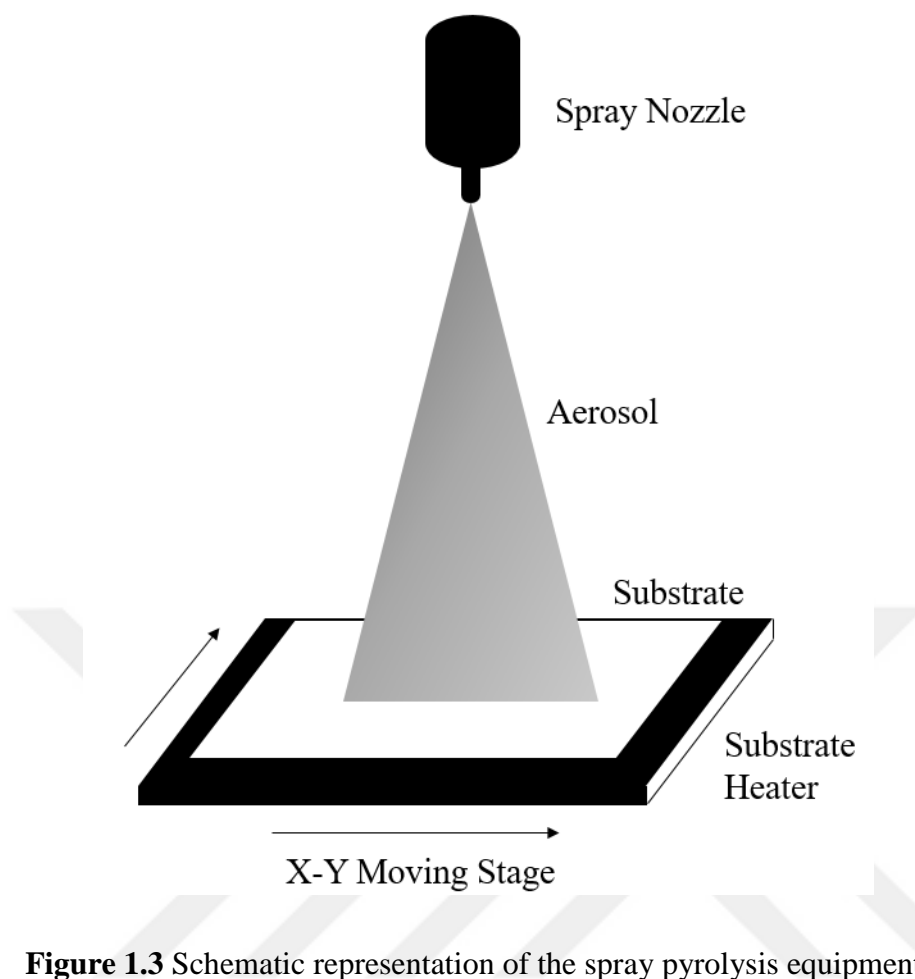


Figure 1.3 Schematic representation of the spray pyrolysis equipment.

Spray pyrolysis equipment consists of a syringe pump, syringe, tube, x-y moving stage, substrate heater and spray nozzle. Equipment should be placed in a fume hood or a sealed ventilated medium to prevent inhalation of hazardous particles. Generally, spray nozzle is located on top of the substrate and aerosol cone is sent perpendicular to the substrate. Depending on the deposited material and device structure, an inclined deposition can also be implemented. For powder and nanoparticle fabrication with spray pyrolysis, a long line between nozzle to substrate is established [15]. In such a setup, heating system is set into the line of aerosol transport to initiate early evaporation and obtainment of particles at the end of the deposition line.

The most significant processing step of spray pyrolysis is the aerosol creation. This is provided by atomization of the precursor solution, which is the fragmentation of incoming stream of liquid into tiny droplets. Gas atomization, ultrasonic atomization and electrostatic atomization are the sources of atomization. When the aerosol reaches the heating zone, solvent of the droplets vaporizes, yielding nanoparticles. These particles build up thin film or larger particles depending on the desired end product [12].

Spray pyrolysis is influenced by many parameters. These parameters are tabulated and provided in Table 1.1. Substrate temperature, nozzle to substrate distance, atomization power, precursor solution, rate of precursor transport and moving stage travel speed are parameters that needs to be optimized to obtain good quality films. As can be seen, there are a lot more parameters to be optimized compared to other solution based deposition methods. Therefore, researchers must put extensive effort to acquire mastership of spray pyrolysis.

Table 1.1 Parameters of the USP system.

PARAMETERS OF THE USP SYSTEM	PARAMETERS OF THE PRECURSOR
<ul style="list-style-type: none"> • Rate of deposition (ml/h) • Amount of deposition (ml) • Distance between nozzle and substrate (cm) • Substrate temperature ($^{\circ}\text{C}$) • X-Y stage motion speed (cm/s) • Annealing temperature ($^{\circ}\text{C}$) 	<ul style="list-style-type: none"> • Viscosity (kg/s.m) • Molarity (M) • Elements of solution

1.2. Transition Metal Oxides

Transition metal oxides are formed by the reaction of oxygen atoms with transition metals. Their unique layered structure are attractive for researchers, because of ease of ion transfer into and out of their structure. These ceramic materials are found in the nature and most of them are non toxic. Formation reactions of metal oxides are effortless and they can be contained in ambient conditions due to being thermodynamically stable. Some extensively investigated metal oxides in literature include WO_3 , MoO_3 , TiO_2 and V_2O_5 . Fabrication of these materials reproducibly in thin film form using different deposition methods enable researchers to improve their performance and compare different methods. Active layers in chromic devices and sensors, charge injection/transport layers of optoelectronic devices are only a few examples where transition metal oxide thin films are utilized.

1.2.1. Molybdenum Oxide (MoO_3)

MoO_3 is a metal oxide that has been widely used due to its unique layered structure and electrochemical active. Mainly, three polymorphs of MoO_3 is investigated. Orthorhombic MoO_3 (α -phase) [21–23], which is thermodynamically stable at standard conditions, monoclinic MoO_3 (β -phase) [19] and hexagonal MoO_3 (h-phase) [20].

As the thermodynamically stable one, α - MoO_3 is the most researched phase. Its crystal structure consists of molybdenum atoms and six fold coordinated oxygen atoms that forms the MoO_6 octahedra. These octahedras are connected to each other by edges, sharing [001] direction that form a zigzag chain. Linked along [100] direction, chains of MoO_3 octahedra form a double-layered sheet that elongates along [010] to form orthorhombic MoO_3 structure [21]. Crystal structure of orthorhombic α - MoO_3 is schematically provided in Figure 1.4.

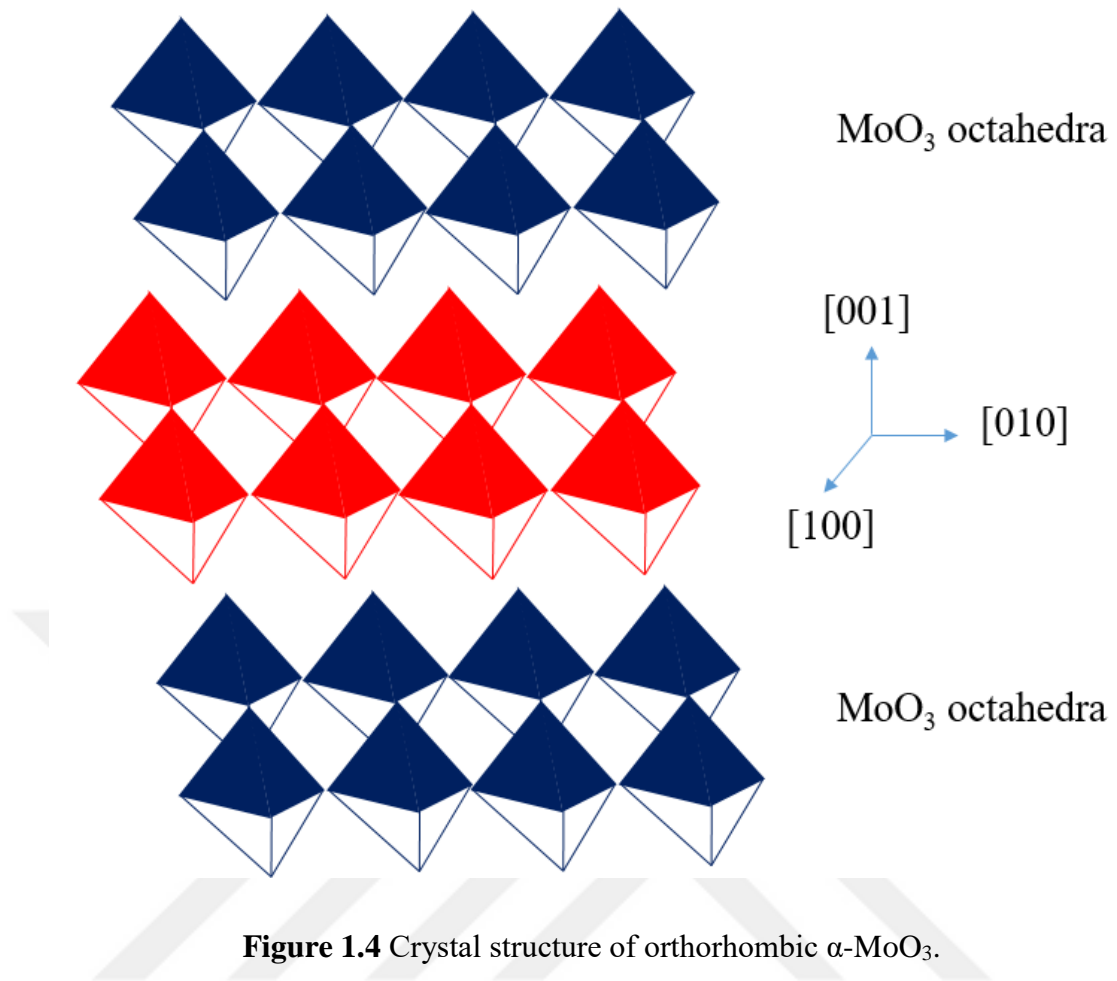


Figure 1.4 Crystal structure of orthorhombic α - MoO_3 .

Thin film α - MoO_3 has been employed as functional layer in many different electronic devices due to its unique characteristics. Favorable energy levels, electrochemical activity, chromic behavior, low cost, non-toxicity, ability to intercalate with ions (such as H^+ , Li^+) and multiple oxidation states are among these characteristics [20–23]. Typical devices include but not limited to, charge generation layer of OLEDs [26], hole-injection layer of organic solar cells [27], electrochromic layers [26–28], hole-extraction layer of polymer solar cells [31], gas sensing layer of formaldehyde sensors [32]. It is also worth noting that MoO_3 is highly promising in optical applications due to a spectral match between its optical absorption peak and the human eye sensitivity [11–13].

A key application of MoO_3 was realized when it is vacuum deposited as thin film and utilized as charge-generation layer of white light emitting stacked organic light emitting diode (SOLED). A SOLED is identical to an organic light emitting diode

(OLED), but with multiple, stacked organic electroluminescent layers, resulting in higher efficiencies. Introduction of a thin MoO₃ charge generation layer to the SOLED device increased the current density and this had a major contribution on the electrophosphorescence efficiency of the device [26]. Resulting phosphorescence graph are given in Figure 1.5.

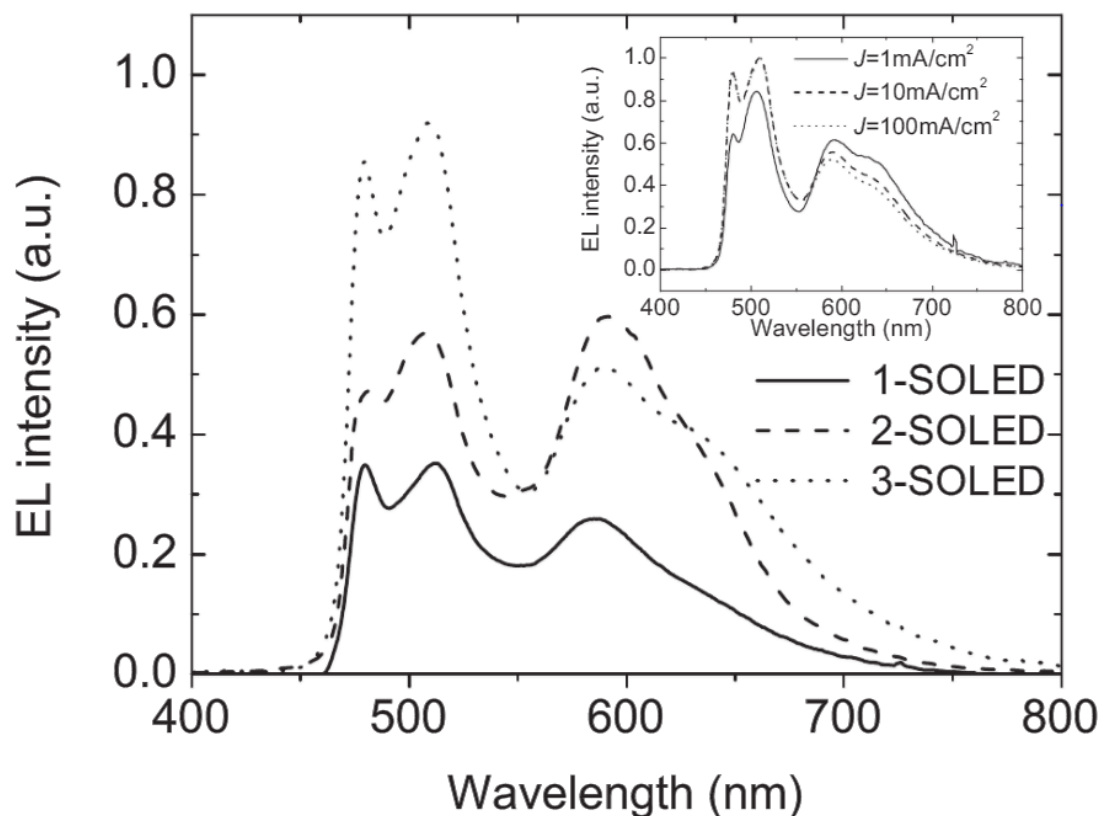


Figure 1.5 Electrophosphorescence spectra of SOLED configurations [26].

MoO₃ thin films were deposited through different methods. Some examples from the literature include spray pyrolysis [34–37], thermal vaporization [38–40], vacuum vaporization [43], atomic layer deposition [44], sputtering [43–45], dip coating [48], electrodeposition [49] and spin coating [21, 48].

Reports suggested that vacuum based and solution based deposition of α -MoO₃ thin films resulted in different oxidation states and work functions [50]. Similar to WO₃ and polyaniline, EC properties of MoO₃ are heavily influenced and depend on the oxidation state of the Mo ion within the MoO₃ structure [51]. Hence, the films

deposited with vacuum and solution based methods likely to differ in terms of coloration efficiency (CE) and stability when utilized in EC devices.

Some studies on solar cells implementing a two-step or sequential deposition (SD) of thin film layers with solution and vacuum based methods have reported promising device performances [23–25]. An improvement in film quality and an increase in charge transport efficiency were reported for the thin films deposited through SD. However, the sequential deposition route is unexplored for the fabrication of EC devices. Therefore, the fabrication of EC devices through sequentially deposited MoO₃ thin films is highly appealing.

1.2.2. Tungsten Oxide (WO₃)

Similar to MoO₃, WO₃ is another transition metal oxide with comparable properties. Its 6-fold octahedral crystal structure is identical to MoO₃. Due to low cost, easy supply and high performance in optoelectronic devices, thin film WO₃ has been extensively utilized in electrochromic devices [53, 54]. It is an indirect bandgap material and shows cathodic electrochromic coloration. Among metal oxides WO₃ is the most researched electrochromic material due to its high transmittance difference between the colored and bleached state (ΔT), CE and cyclic stability [55, 56]. Deposition of WO₃ thin films for electrochromic device applications by both solution [57–59] and vacuum based [63] methods have been investigated in detail. In addition to electrochromics, thin film WO₃ have also been employed as charge injection layer in solar cells [64–66]. In another study, WO₃ and MoO₃ are deposited sequentially and an enhanced gas sensing performance was reported for this multilayer film [67].

1.2.3. Titanium Oxide (TiO₂)

TiO₂ is the thermodynamically stable oxide phase of titanium at standart conditions. Being mainly used in industry for coloring, it has some distinct applications. TiO₂

attracted recent attention due to its photocatalytic activity in dye-sensitized solar cells [64–66]. There are four known polymorphs of TiO₂, which are rutile (tetragonal), anatase (tetragonal), brookite (orthorhombic) and monoclinic B-phase TiO₂ [71]. In many applications, TiO₂ was synthesized and employed as nanoparticles. It was reported that application of TiO₂ nanoparticles has shown enhanced photocatalytic activity compared to thin film TiO₂ [72]. In addition, application of TiO₂ in various morphologies as EC device has also been successful in terms of EC performance [69–72].

1.3. Electrochromic (EC) Devices

Electrochromism is defined as the reversible color (transmittance) change through the application of an external voltage [77]. Utilization of electrochromic (EC) devices as smart windows in buildings is suggested to lower the energy consumption [78]. Both inorganic and organic materials were employed as an electrochrome layer [79]. There are two types of electrochromism, namely cathodic and anodic. Oxides of Ti, Mo, Nb, Ta and W are found to exhibit cathodic coloration. On the other hand, oxides of elements Cr, Mn, Fe, Co, Ni, Rh and Ir exhibit anodic coloration. Transition metal elements with cathodic and anodic electrochromic oxides are given in Figure 1.6.

ELECTROCHROMIC OXIDES:

H																			He	
Li	Be														B	C	N	O	F	Ne
Na	Mg														Al	Si	P	S	Cl	Ar
K	Ca	Sc	Ti	V	Cr	Mn	Fe	Co	Ni	Cu	Zn	Ga	Ge	As	Se	Br	Kr			
Rb	Sr	Y	Zr	Nb	Mo	Tc	Ru	Rh	Pd	Ag	Cd	In	Sn	Sb	Te	I	Xe			
Cs	Ba	La	Hf	Ta	W	Re	Os	Ir	Pt	Au	Hg	Tl	Pb	Bi	Po	At	Rn			
Fr	Ra	Ac																		

Cathodic coloration
Anodic coloration

Figure 1.6 Elements of the periodic table with electrochromic oxides. Type of electrochromism is provided in the legend [86].

Electrochromic transition occurs by a process termed as intercalation. By this process, electrochrome metal reacts with the ion in the medium, which comes from the electrolyte. Reaction occurs due to an applied voltage. Similarly, when the polarity of the voltage is reversed transmittance of the device must turn back to its initial value. This is termed as deintercalation. To make intercalation and deintercalation possible, thin film must be in contact with a conductive layer for the voltage and the electrolyte for the ions. For the most typical use of electrochromic devices, smart windows, a transparent conductive layer is deposited onto a glass substrate. Electrochrome layer is then deposited onto the transparent conductive layer. In industrial applications, a symmetric layer is also formed and the electrolyte is sandwiched between them. For the opposite layer, an ion storage film is used and its coloration is opposite to the electrochrome material. Such a device is called a full cell and it is schematically shown in Figure 1.7.

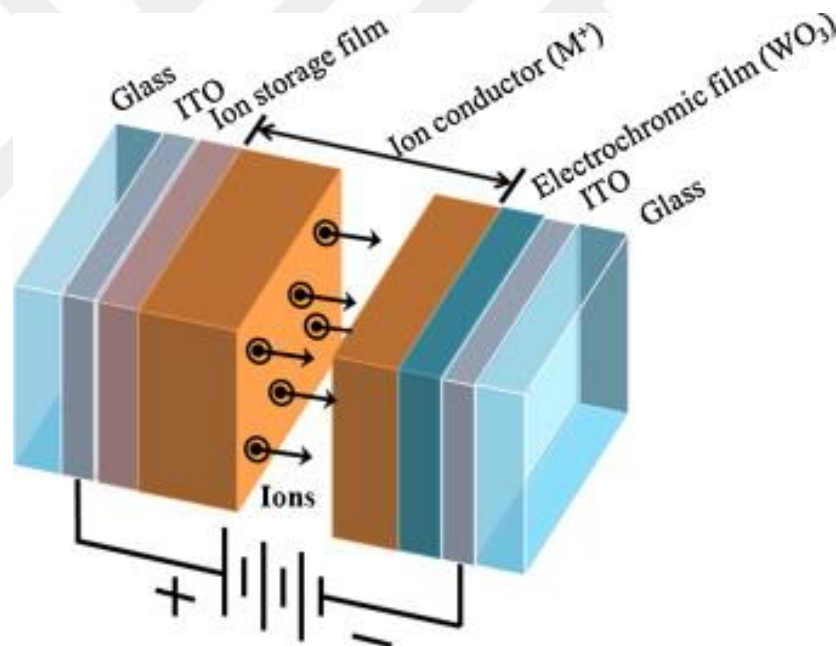


Figure 1.7 A full cell electrochromic device based on WO₃ and ITO [85].

Among inorganic electrochrome materials, WO₃ is the most widely used one. WO₃ based EC devices have shown high coloration efficiency, fast switching and promising long term stability [4–6]. Electrochromic applications of MoO₃ and WO₃

date back to 1960s [43, 82]. Until recently, most of the studies on WO_3 electrochromism was based on amorphous thin films with disordered structure. Researchers used to believe that such a structure yields higher EC performance as opposed to crystalline counterparts. To fabricate crystalline WO_3 , sputtering technique was employed in literature, while amorphous films were deposited via thermal evaporation without any post deposition process [83]. But then, EC devices based on crystalline WO_3 were reported to show high coloration efficiencies ($42 \text{ cm}^2 \text{ C}^{-1}$) and they were much more stable than amorphous WO_3 based ECs. An important factor in this study was the fabrication of WO_3 layer as crystalline nanoparticles [57]. Since most of the applications of ECs demand high stability under cyclic transformation, crystalline transition metal oxide fabrication has been favored against amorphous thin films [84]. When compared to WO_3 , MoO_3 is a relatively unexplored material in terms of an EC device due to its lower coloration efficiency.

Although not as popular as WO_3 , EC devices based on MoO_3 thin films have also been researched. Deposition of MoO_3 have been conducted by various precursor compositions. Ammonium molybdate tetrahydrate ($(\text{NH}_4)_6\text{Mo}_7\text{O}_{24} \cdot 4\text{H}_2\text{O}$) is one such precursor for the deposition of MoO_3 thin films. In a work employing $(\text{NH}_4)_6\text{Mo}_7\text{O}_{24} \cdot 4\text{H}_2\text{O}$, fluorine doped tin oxide (FTO) coated glass was used as the substrate for the electrodeposition of MoO_3 thin films. As a post deposition process, films were annealed at 450°C . Top-view SEM images of the as deposited and annealed thin films are provided in Figure 1.8. Nanorod like features were observed to occur in the film that is subjected to annealing. Optical transmittance of the films was measured after coloration. Bleached state transmittance value was observed to be reported from the initial transmittance value, although it should have been reported from the transmittance value of the uncolored film after coloration state. Generally, the state before coloration is termed as initial or virgin state of the device. By calculating CE from the transmittance difference between initial and colored states, a resulting value of $34 \text{ cm}^2 \text{ C}^{-1}$ was obtained [87].

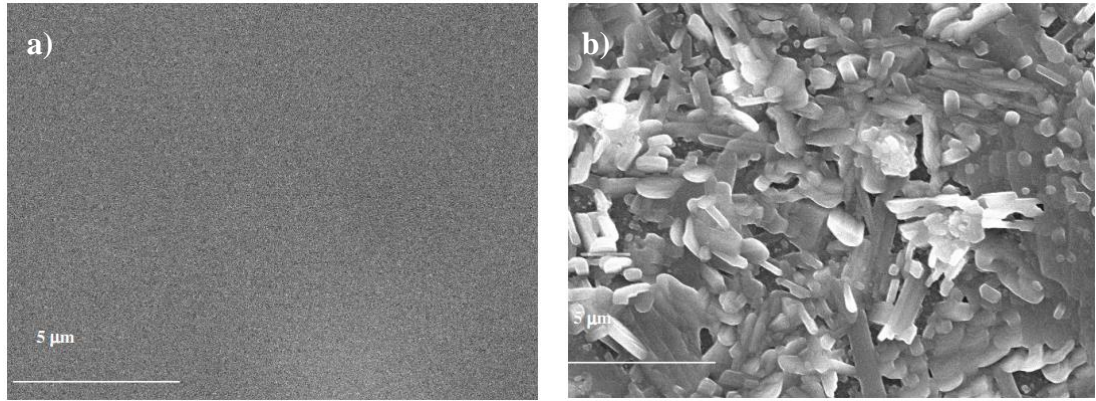


Figure 1.8 SEM images of the (a) as deposited and (b) annealed (450°C) films prepared by electrodeposition [87].

In another work, deposition of MoO_3 thin films for EC application was performed with sol-gel spin coating technique. For this purpose, metallic molybdenum powder was dissolved in hydrogen peroxide (H_2O_2) and acetic acid (CH_3COOH) was added as a surfactant. Deposition was carried out onto indium tin oxide (ITO) coated glasses and prepared thin films were annealed at 100, 200, 300, 350, 400 and 500°C for 1h. Thickness of these films were 700 nm. Top-view SEM images of the films is given in Figure 1.9 [28].

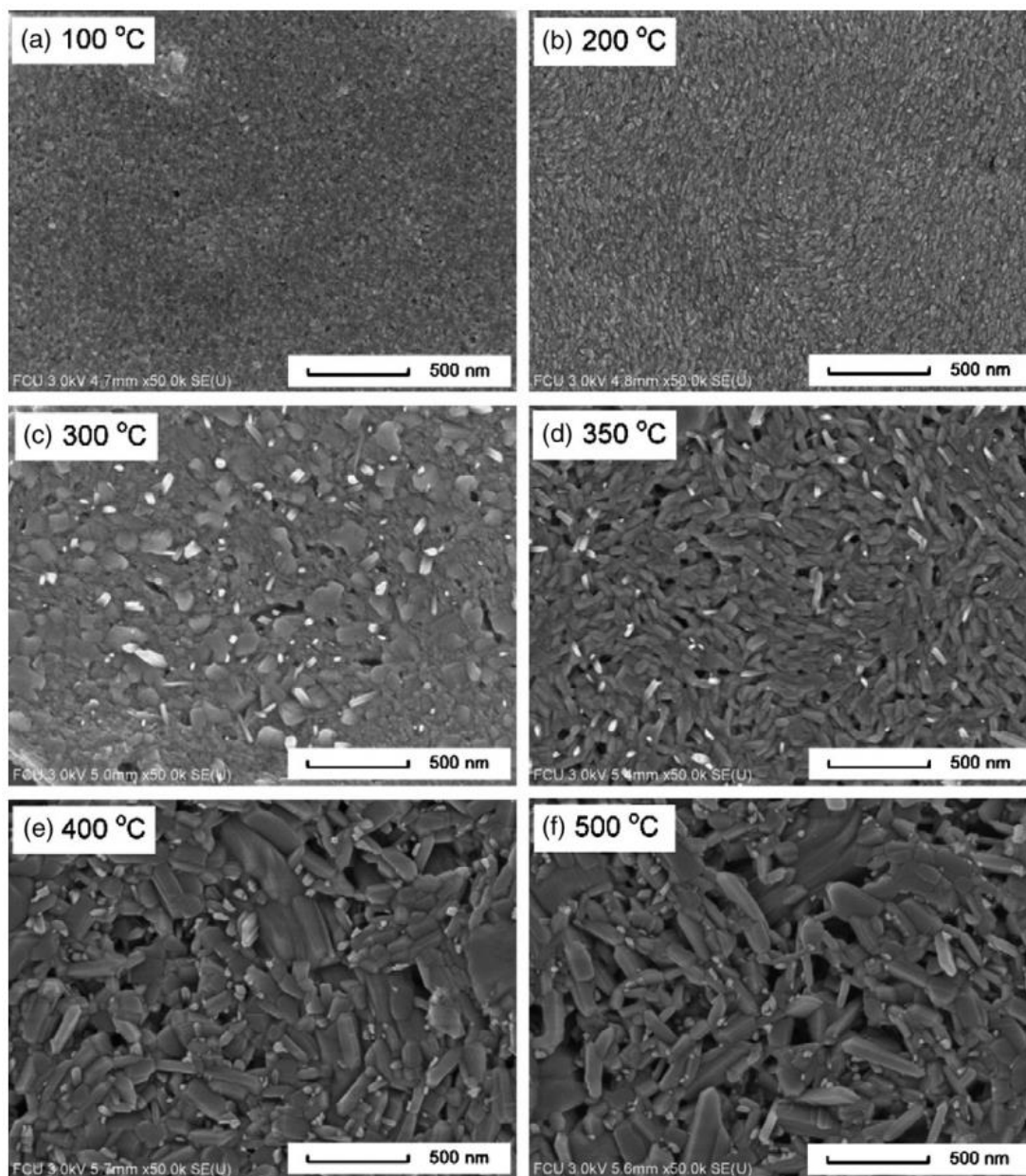


Figure 1.9 SEM images of the MoO₃ thin films annealed at (a) 100, (b) 200, (c) 300, (d) 350, (e) 400 and (f) 500°C [28].

Although no additional information was given for the high temperature compatibility of glass and ITO used in the system, EC performance was reported for the films annealed at temperatures of 500°C. In general, ordinary glass cannot endure such a high temperature. To conduct a fabrication with high post annealing temperatures, glass substrates with specific compositions should be used and it would add to the

cost of the devices. Independent from this fact, CE values of the sample annealed at 500°C were reported as the highest CE for the thin film MoO₃ in recent publications [88]. Also ΔT and CE measurement at a wavelength of 900 nm has no practical meaning due to being out of visible spectral zone. This is because the major application of EC devices is the smart windows, which operates within the visible region (400-700 nm) of the optical spectra. EC performances obtained in this work are given in Table 1.2. Maximum CE values of the samples annealed below 500°C were 23.7 cm² C⁻¹ and 44.9 cm² C⁻¹ at wavelengths of 550 nm and 700 nm, respectively, within the visible region [28].

Table 1.2 EC performance of the MoO₃ thin films at different annealing temperatures [28].

Annealing temperature		100 °C	200 °C	300 °C	350 °C	400 °C	500 °C
Inserted charge density, Q_c (mC/cm ²)		1.4	12.7	13.9	15.8	12.7	12.6
Extracted charge density, Q_a (mC/cm ²)		0.5	9.8	11.0	14.5	11.0	11.1
Q_c/Q_a ratio		2.80	1.30	1.26	1.09	1.15	1.14
$\lambda=550$ nm	$T_{bleached}$	79%	83%	80%	80%	67%	64%
	$T_{colored}$	75%	78%	37%	35%	36%	32%
	ΔT	4%	5%	43%	45%	31%	32%
	ΔOD	0.02	0.03	0.33	0.36	0.27	0.30
	CE (cm ² /C)	14.3	2.4	23.7	22.8	21.3	23.8
$\lambda=700$ nm	$T_{bleached}$	82%	86%	87%	86%	71%	67%
	$T_{colored}$	81%	74%	25%	21%	19%	17%
	ΔT	1%	12%	62%	65%	52%	50%
	ΔOD	0.01	0.07	0.54	0.61	0.57	0.60
	CE (cm ² /C)	7.1	5.5	38.8	38.6	44.9	47.6
$\lambda=900$ nm	$T_{bleached}$	79%	81%	82%	80%	64%	58%
	$T_{colored}$	77%	56%	28%	15%	14%	12%
	ΔT	2%	25%	54%	65%	50%	46%
	ΔOD	0.01	0.16	0.47	0.73	0.66	0.68
	CE (cm ² /C)	7.1	12.6	33.8	46.2	52.0	54.0

Recently, utilization of MoO_3 thin films with and as an additive to the other transition metal oxides are investigated. TiO_2 is one such example used with MoO_3 , where enhanced optical density (ΔOD) and stability were reported for this binary system [89, 90]. In another example, thin film MoO_3 was electrodeposited onto sputtered niobium oxide (Nb_2O_5) thin films again for electrochromic applications. To conduct MoO_3 deposition onto Nb_2O_5 thin films, a precursor was prepared with sodium molybdate (Na_2MoO_4) and distilled water. A parametric study regarding the deposition of MoO_3 with different number of deposition cycles was performed. Top-view and cross-sectional SEM images of the samples are provided in Figure 1.10.



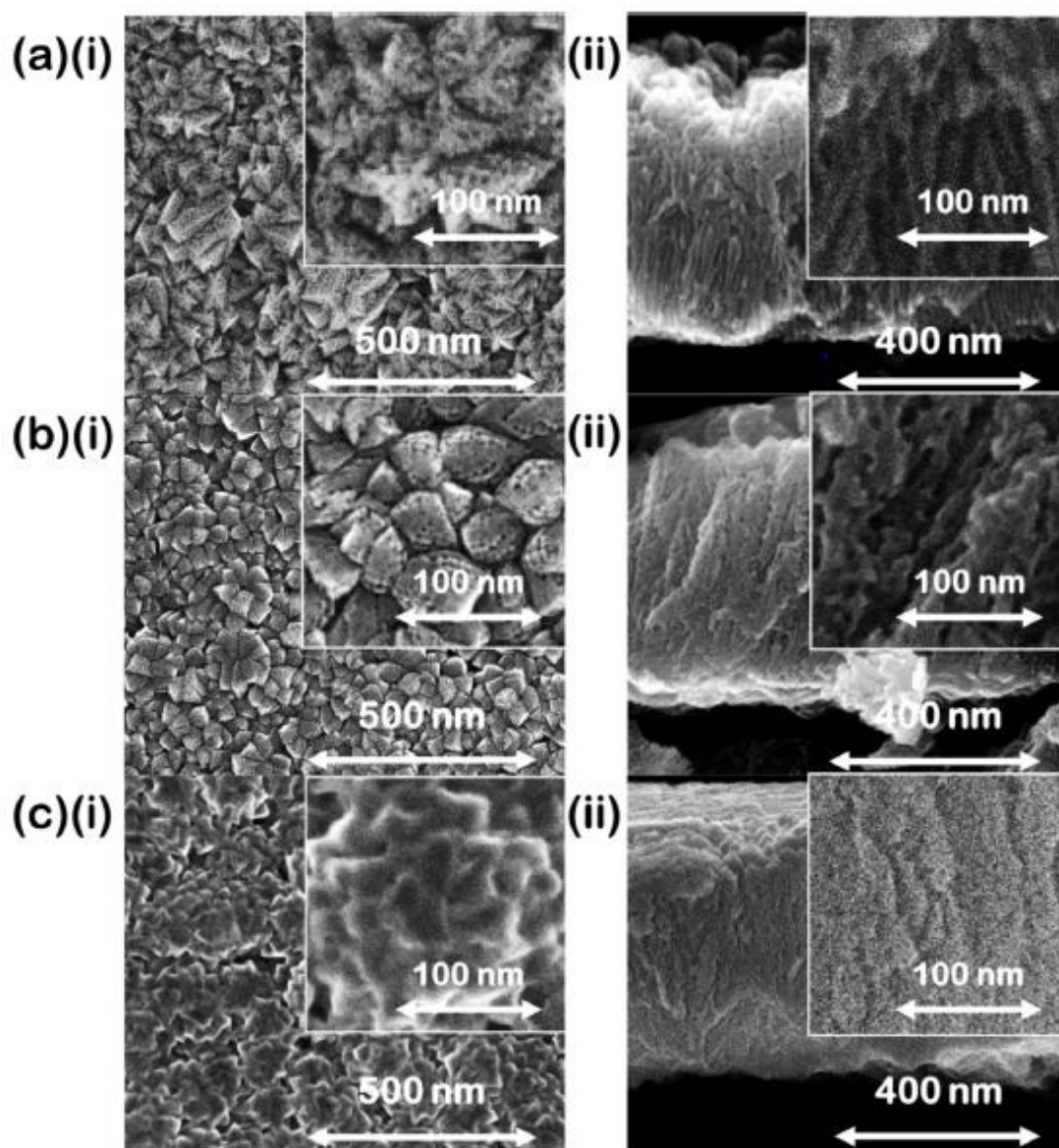


Figure 1.10 Top-view (i) and cross-sectional (ii) SEM images of the (a) bare Nb_2O_5 and MoO_3 , (b) 40 cycles and (c) 120 cycles [88].

CE of the deposited binary system were calculated for MoO_3 deposition cycles of 20, 40, 80 and 120. Initial values of $10\text{-}20\text{ cm}^2\text{ C}^{-1}$ CE were increased to $149\text{ cm}^2\text{ C}^{-1}$, found as the maximum CE for 120 cycle deposited thin film MoO_3 [88]. Spectroelectrochemical performance of the samples with different MoO_3 deposition cycles are given in Figure 1.11.

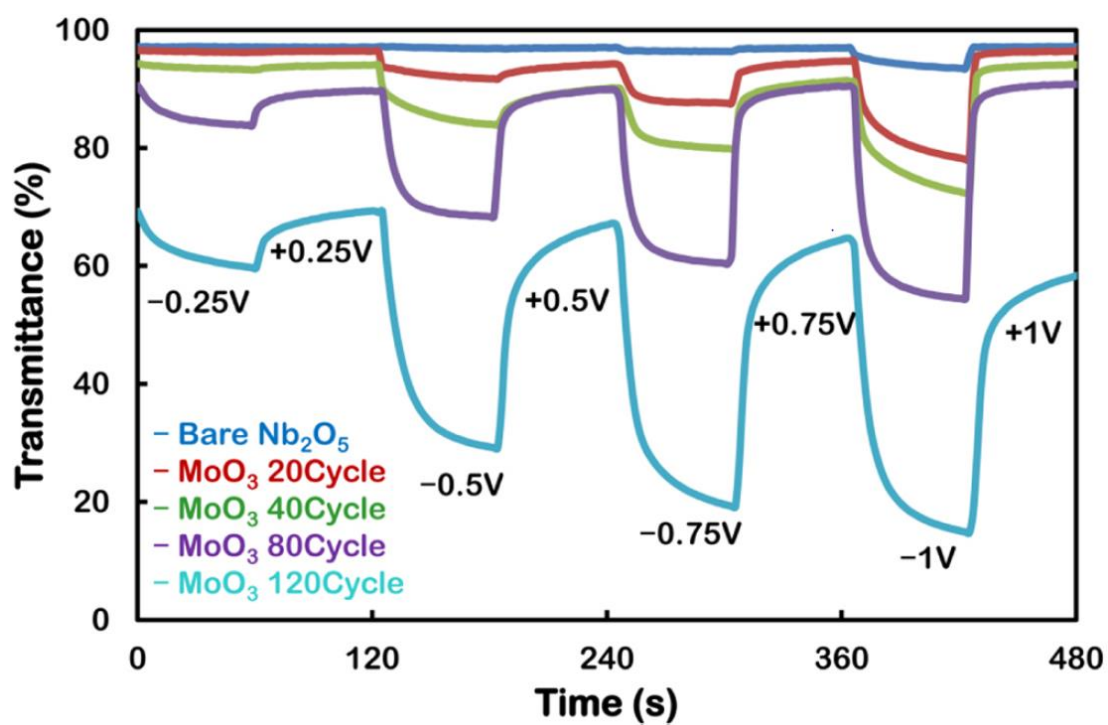


Figure 1.11 Kinetic transmittance change of the samples at the applied voltages from ± 0.25 to 1.00 V [88].

In this work, USP and thermal evaporation methods are used for the fabrication of MoO₃ coated ITO electrodes. Sequential deposition by combination of these two techniques is also used to investigate the resulting performance of the EC electrodes.

CHAPTER 2

EXPERIMENTAL DETAILS

2.1. Ultrasonic Spray Pyrolysis (USP) System

A custom USP setup was prepared and utilized for the deposition of thin films. In this setup, an ultrasonic atomizer nozzle (PNR B1 0103) was connected to a syringe pump (TOP-5300) through a silicone pipe for precursor transfer. Ultrasonic atomization was initiated through nitrogen (N_2) gas at a flow rate of 90 ml/h. Atomization of the precursor was materialized by two steps:

- 1) Incoming precursor was transferred into the nozzle and atomization was conducted by shearing. High pressure air mixes with the precursor and pushes it through the nozzle outlet orifice.
- 2) High speed atomized precursor then impacts onto the resonator device placed in front of the nozzle to generate ultrasonication. By this process, a hybrid atomization is carried out.

A hot plate carrying the substrate was placed onto a moving xy-stage for the deposition of uniform thin films. Our current moving stage covers an area of 30 cm x 40 cm. However, substrate heater acts as the rate limiting factor, and makes it possible to deposit an area smaller than it. Energy required for the movement of the plates carrying the substrate in x- and y- directions is given by an external power supply. X-direction of the moving stage is programmed to exhibit turning back motion when it reaches to the end of the line. At the end of each x-direction movement, stage moves 1 cm in y-direction. Direction of movement in y-axis is controlled manually by switching the polarity of the voltage. Applied voltage to rotating motors under the plates conduct movements at x- and y-direction were 8 and

14 V respectively. The whole setup was built in a fume hood for proper ventilation during deposition. A photograph of the USP system is given in Figure 2.1.

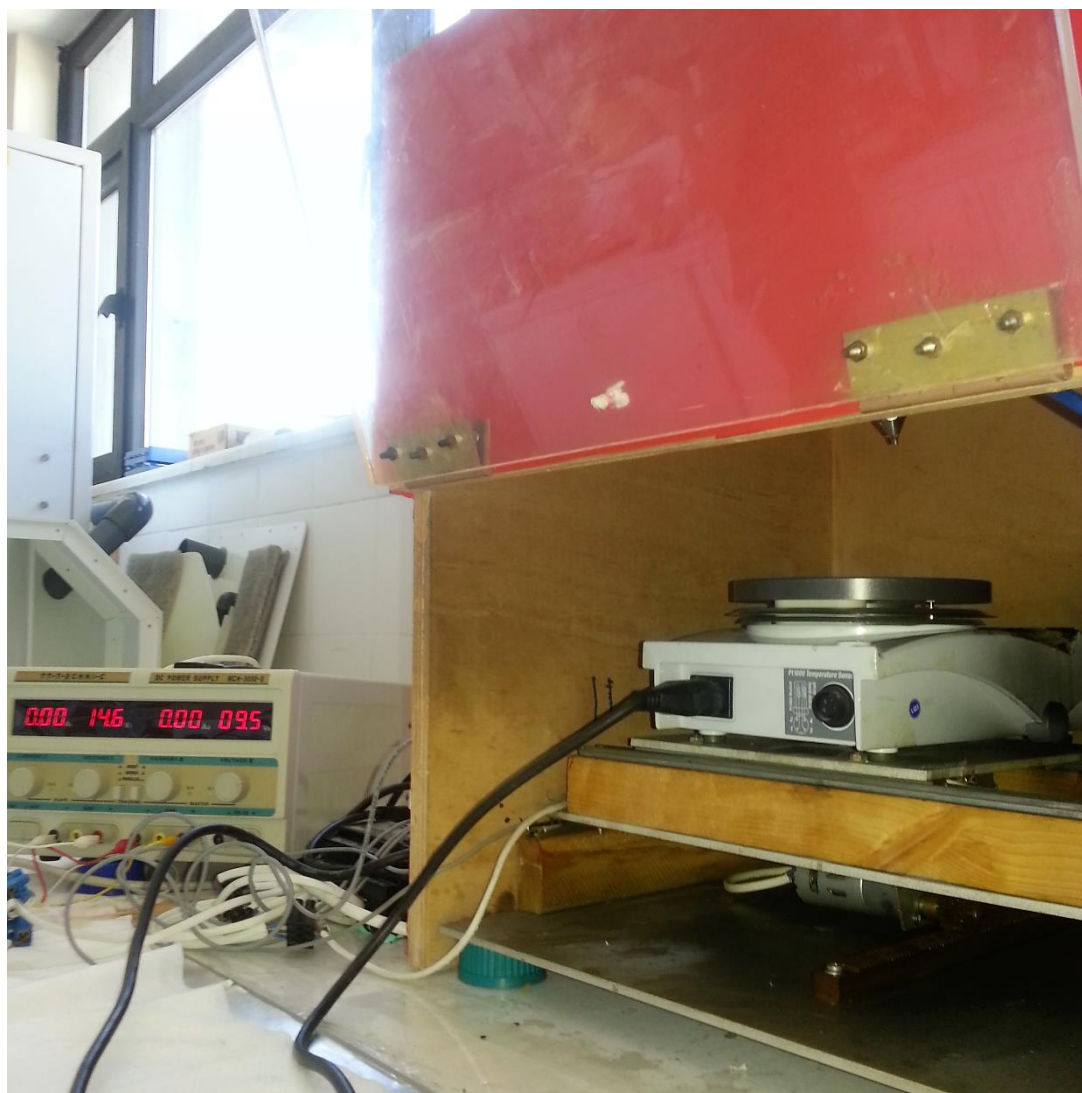


Figure 2.1 Photograph of the home made USP system.

2.2. Deposition by USP

Molybdenum chloride (MoCl_5 , 95% in purity, Sigma-Aldrich) was dissolved in ultra-pure (UP) water (18.3 M Ω). Dissolution process was performed in a fume hood due to the formation of a strong acidic gas according to the following reaction:



Prior to the deposition of thin films, precursor was ultrasonicated to accelerate the dissolution. Afterwards, the precursor was transferred to the deposition system by a 25 ml syringe. Substrate temperature was set to 300°C. The deposition rate and nozzle to substrate distance was set to 90 ml/h and 40 cm, respectively. Such a high nozzle to substrate distance was used to prevent the reach of droplets to the substrate. A photograph of prepared precursors is provided in Figure 2.2. A color variation is observed for each molarity.



Figure 2.2 Precursor solutions prepared by dissolving MoCl_5 in UP water. Molarities of the solutions from left to right are 1, 5 and 10 mM respectively.

2.3. Deposition by Thermal Evaporation

Molybdenum oxide thin films (MoO_3 , 99.97% in purity, Sigma-Aldrich) were also deposited by thermal evaporation. Since MoO_3 was in powder form, voltage applied to evaporation boats was slowly raised to prevent its uncontrolled evaporation, which

would otherwise lead to the deposition of a non-homogeneous film. Deposition was performed at a rate of 1.5 Å/s on rotating substrates to improve film homogeneity. In order to obtain high purity thin films, evaporation was started at a base pressure of 2×10^{-6} torr.

2.4. Sample Preparation

Deposition was performed on glass substrates (1.27 x 2.54 cm) and on ITO coated glass slides ($50 \Omega/\text{cm}^2$) (0.5 cm x 5.0 cm). Both substrates were cleaned through ultrasonication in acetone, isopropanol and UP water, consecutively, for 10 minutes each. Films with different thicknesses were deposited and annealed prior to characterization. 4 samples were prepared and named as the follows. First sample, named as USP-A, was deposited and annealed at 400°C. Second sample prepared by thermal evaporation was named as PVD. The third sample prepared by the same route but annealed afterwards at 400°C was named as PVD-A. The last sample prepared by USP followed by thermal evaporation and annealing at 400°C was named as SD-A. EC devices were fabricated using thin films deposited onto ITO coated glass substrates. Photograph of USP deposited samples are given in Figure 2.3. Sample designations and descriptions are provided in Table 2.1. Deposition was performed on ITO coated glass substrates. By masking the samples during deposition, desired visuals can be obtained.

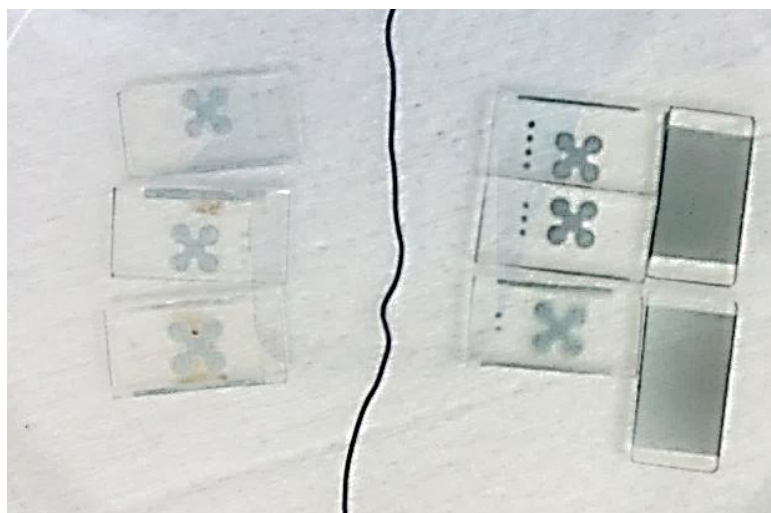


Figure 2.3 A photo showing various samples deposited by USP method on ITO coated glass substrates.

Table 2.1 Designations and descriptions of the samples.

SAMPLE	DEPOSITION METHOD	ANNEALING
PVD	Thermal evaporation	Not annealed
PVD-A	Thermal evaporation	400°C and 1 hour
USP-A	USP method	400°C and 1 hour
SD-A	SD method	400°C and 1 hour

2.5. Characterization and EC Characteristics

XRD method was employed to investigate the crystal structure and chemical composition of the deposited thin films. For this purpose, a Rigaku D/Max-2000 diffractometer was used at Bragg-Brentanno geometry with Cu $K\alpha$ radiation operating at 40 kV. Diffraction angle was varied between 10 and 90° at a scan speed of 1°/min. Surface morphology and topography of the films were analyzed by

atomic force microscopy method (AFM) using a Veeco MultiMode V instrument under tapping mode. For AFM measurements, size of the coated glasses was reduced to 1 cm x 1 cm. X-Ray photoelectron spectra (XPS) were collected using a PHI 5000 versaprobe spectrometer. 284.5 eV line of C (1s) was used as a reference value for charge correction. Scanning electron microscopy (SEM, FEI Nova Nano FEG-SEM 430, operated at 10 kV) was also utilized for the morphological analysis of the deposited thin film surface. A few nanometers of gold were sputtered prior to SEM analysis. Spectroelectrochemical studies of thin films were carried out using a Varian Cary 5000 UV–Vis spectrophotometer with lithium perchlorate (LiCl_4) electrolyte. Cyclic voltammetry measurements of the EC devices were conducted using a Gamry Reference 600 potentiostat.



CHAPTER 3

RESULTS AND DISCUSSION

3.1. Optimization of USP method

Optimization of USP deposition was performed by pilot studies. As stated before, system has many parameters and deposition of thin films involved optimization of these parameters. Most of the optimization was carried out by macroscopic inspections. In order to deposit MoO_3 thin film by USP method, first step was to determine the correct molybdenum salt. Ammonium molybdate was commonly utilized in literature. However, initial trials using ammonium molybdate in our USP system did not result in the formation of MoO_3 thin films. Insufficient heating might simply be the reason for this. The use of chloride salts for the formation of metal oxides is quite common and is extensively used for the deposition of WO_3 . Therefore, right after ammonium molybdate, molybdenum chloride (MoCl_5) was used as the salt for the deposition of MoO_3 thin films. Initial trials with MoCl_5 was successful and thus further experiments were conducted using this salt.

Next step was to optimize the solution concentration. For this purpose, precursors with different molarities (1, 5, and 10 mM) were prepared. In all of the precursor solutions, agglomerate formation was observed after some time. Rate of agglomeration was the slowest for 1 mM solution and because of this reason it was used for the depositions. For concentrations lower than 1 mM, rate of deposition (increase in thickness) was too low and the overall deposition became impractical.

As for solvent selection for the preparation of the precursor solution, ethanol and UP water were compared. MoO_3 thin films deposited using ethanol as a solvent did not show EC response; thus, UP water was decided to be used as the solvent.

Thickness of the thin films determined their transparency. Films with thicknesses higher than 200 nm have shown low optical transmittance for EC electrodes.

Substrate and annealing temperature of the thin films were evaluated by various methods. For the substrate temperature, SEM and macroscopic imaging were used. In general, when the substrate temperature is insufficient, droplets reach to the substrate. If this happens, oxidation of precursor does not reach to completion and surface of the thin film becomes rough. For high substrate temperatures, evaporation of the droplets occurs earlier and particles form over the substrate and reach to the surface. These particles may even be too large to disrupt the film formation. Annealing temperature was evaluated in the range of 300-500°C. Films below 400°C did not show EC response and for those annealed over 400°C, substrate glass and transparent conductive layer was observed to be damaged. Effect of parameters on the end product of the USP deposition is given in Figure 3.1. Following these pilot experiments for the optimization of USP parameters, deposited thin films were structurally characterized and their EC performance was evaluated.

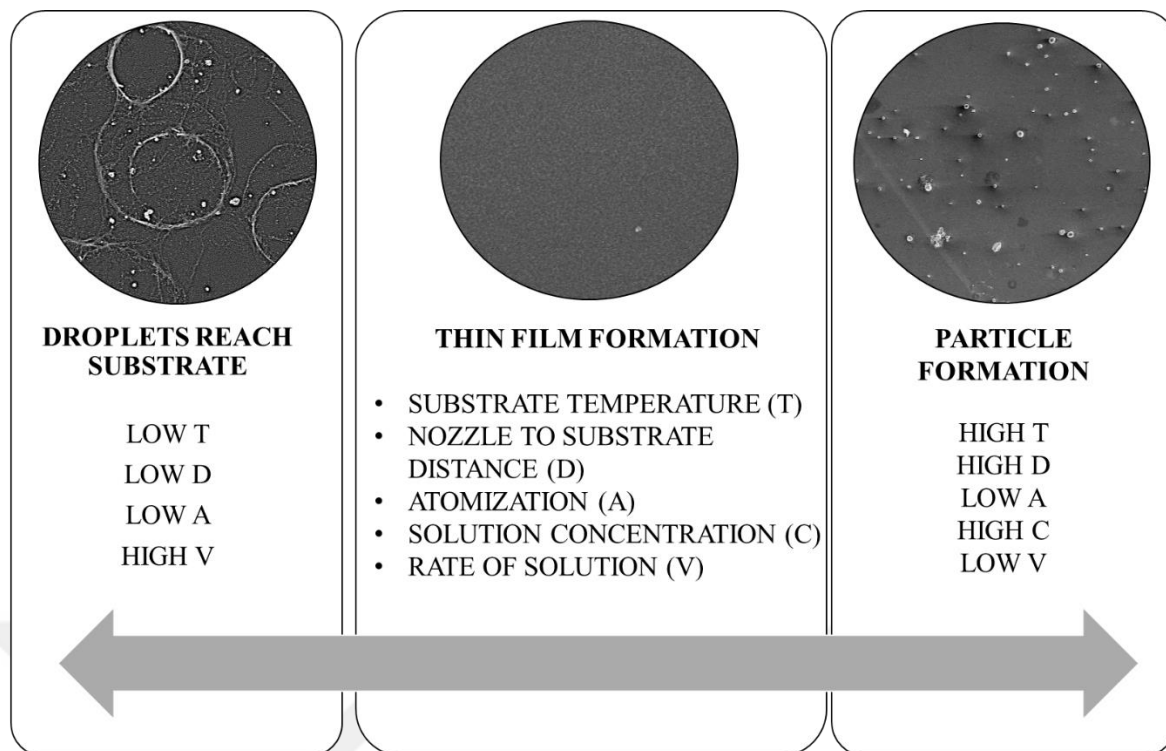


Figure 3.1 Effect of USP parameters on the end product and SEM images collected from such cases.

3.2. Characterization

3.2.1. XRD Measurements

XRD pattern of the samples PVD, PVD-A, USP-A and SD-A are provided in Figure 3.2. Na-PVD sample was observed to have an amorphous nature, due to the absence of any sharp peaks. Pattern for the USP-A sample contain sharp peaks at 13, 26 and 48°, which can be attributed to the diffraction from (020), (040) and (002) planes of stoichiometric MoO₃, respectively. Upon annealing the film deposited by thermal evaporation, sharp peaks were formed as shown in the XRD pattern of the PVD-A sample. This points out the crystallization of the film layer through annealing. As will be shown later, EC performance improves upon crystallization, since ions that conduct electrochromic transformation recites in the octahedral sites of crystalline

MoO₃ structure [86]. For the SD-A sample diffraction pattern, peaks originated from PVD-A was traceable. On the other hand, sharp peaks of high intensity at diffraction angles of 24, 26 and 28° can be attributed to (110), (040) and (021) planes of stoichiometric MoO₃, respectively (JCPDS card No: 05-0508).

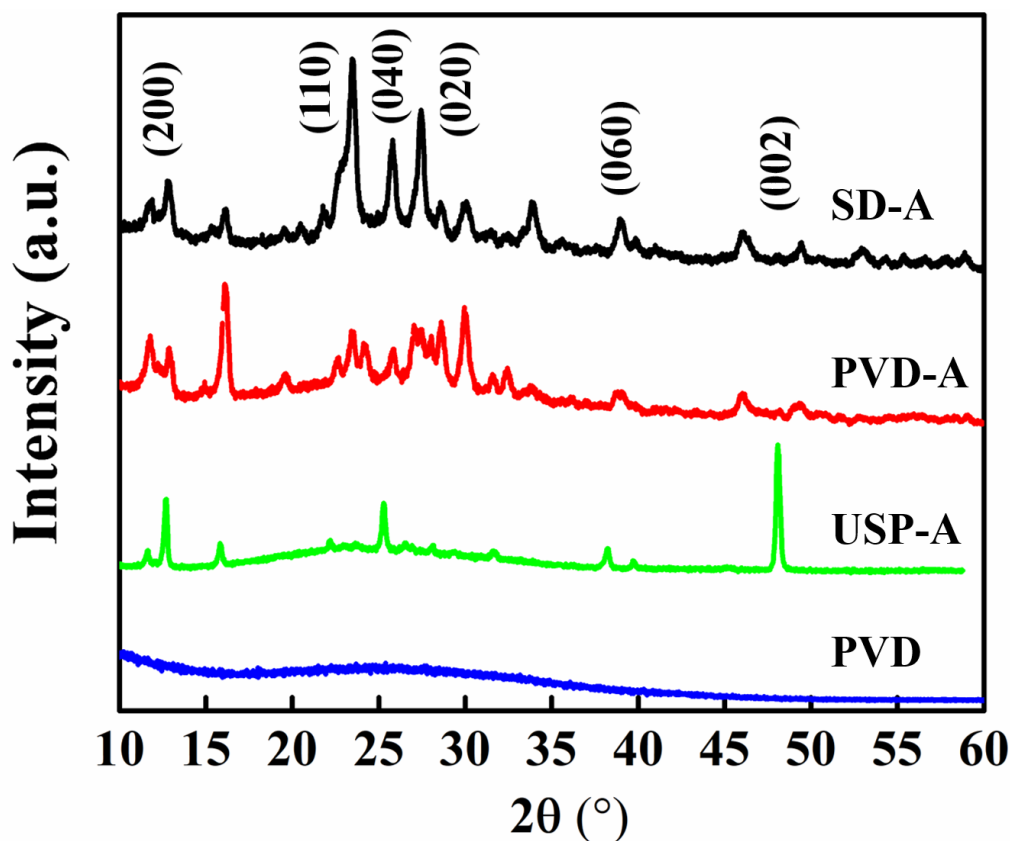


Figure 3.2 X-ray diffraction pattern of the samples (JCPDS card No: 05-0508).

3.2.2. XPS Measurements

XPS analysis was carried out to further characterize the film and determine the oxidation state of Mo. Survey spectra of SD-A is provided in Figure 3.3.

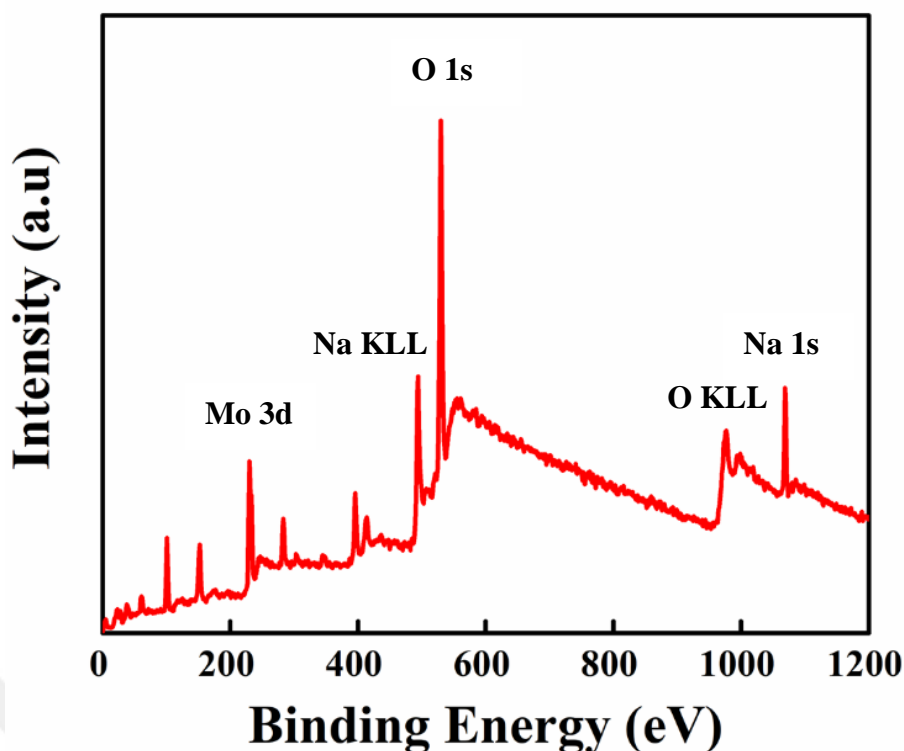


Figure 3.3 Survey spectra of SD-A sample.

Mo 3d and O 1s core level XPS peaks are provided in Figures 3.4 (a) and (b) respectively. Binding energy of Mo 3d peaks are characteristic and used to identify the presence of oxide phase within the structure. In Figure 3.4 (a), Mo 3d core level spectra of the samples are shown. The doublet separation energy of each sample is 3.1 eV and it is characteristic to MoO₃ [91]. Binding energy of Mo 3d 5/2 peak of stoichiometric MoO₃ has been previously reported as 232.5 eV [84, 85]. Stoichiometric MoO₃ structure contains dominance of Mo⁺⁶ ions relative to Mo⁺⁵ and Mo⁺⁴ and from the obtained results, we expect a similar structure for SD-A sample. On the other hand, binding energy of 3d 5/2 peak of PVD sample has a comparable value (232.6 eV), which indicates a similar valence composition of Mo atoms in the structure. Similarity of SD-A and PVD-A samples in terms of XPS results was expected, since thermal vaporization was used to deposit the outmost layer of both samples and XPS is a surface sensitive method with low penetration depth [94]. Mo 3d doublets of USP-A sample are located at 232.1 eV, which points out lower oxidation states within the structure. The value of Mo⁺⁴ and Mo⁺⁵ states

was found to be 229.5 and 231.0 eV, respectively [93]. Binding energy differences of 2.6 eV and 1.1 eV of Mo 3d 5/2 peak of USP-A sample with lower oxidation states suggested that Mo⁺⁶ has the relatively highest concentration among the other oxidation states. A slight difference of 0.2 eV between PVD and PVD-A samples showed that no significant change in terms of oxidation state or chemical structure was recorded following annealing of the thermally evaporated sample. In Figure 3.4 (b), O 1s core level spectra of the samples are provided. For stoichiometric MoO₃, O 1s peak should be located within 530-531 eV range [24]. For the USP-A sample, the peak is shifted towards higher binding energies, which could have been caused by an impurity among the structure. Presence of lower oxidation states of Mo or utilization of UP water as the solvent, which produces –OH bonding among the structure, may be responsible for the shift of O 1s peak towards higher energies [95]. For SD-A sample, existence of a high intensity doublet was observed. The reason behind this cannot be double spin of the electrons emitted, since O 1s peak is single for MoO₃. The intensity of the additional peak is too high to be caused by contamination. Intensity of both peaks of the SD-A sample are nearly equal. Comparison of the binding energy values of SD-A sample peaks (532.4 and 530.4 eV) with other samples shows that these peaks are originated from USP and thermal evaporation deposited parts of the sample. From this data, it can be said that SD method produces two separate phases of MoO₃ that shows different binding energies.

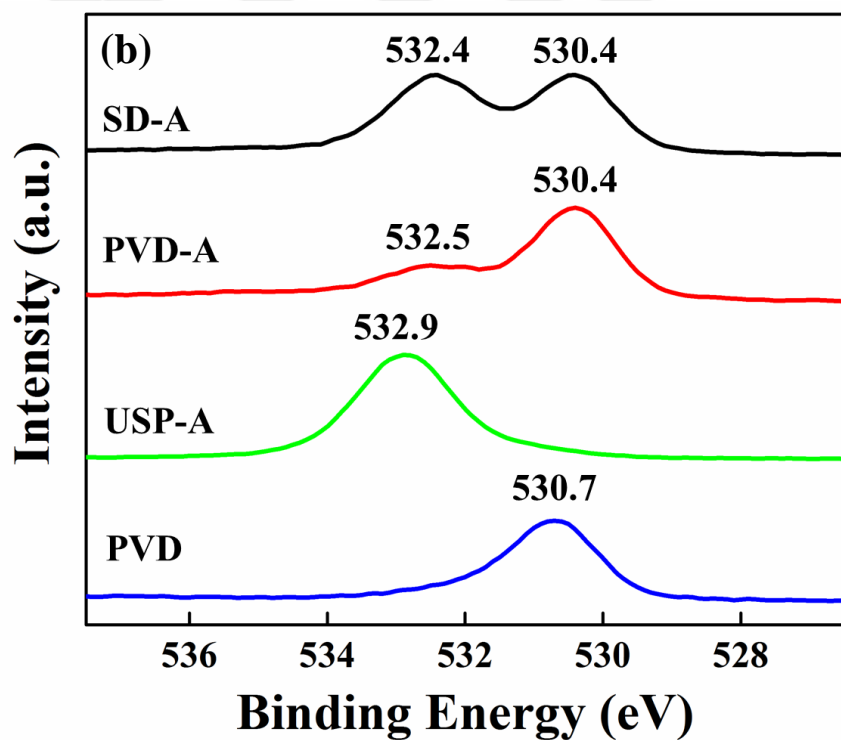
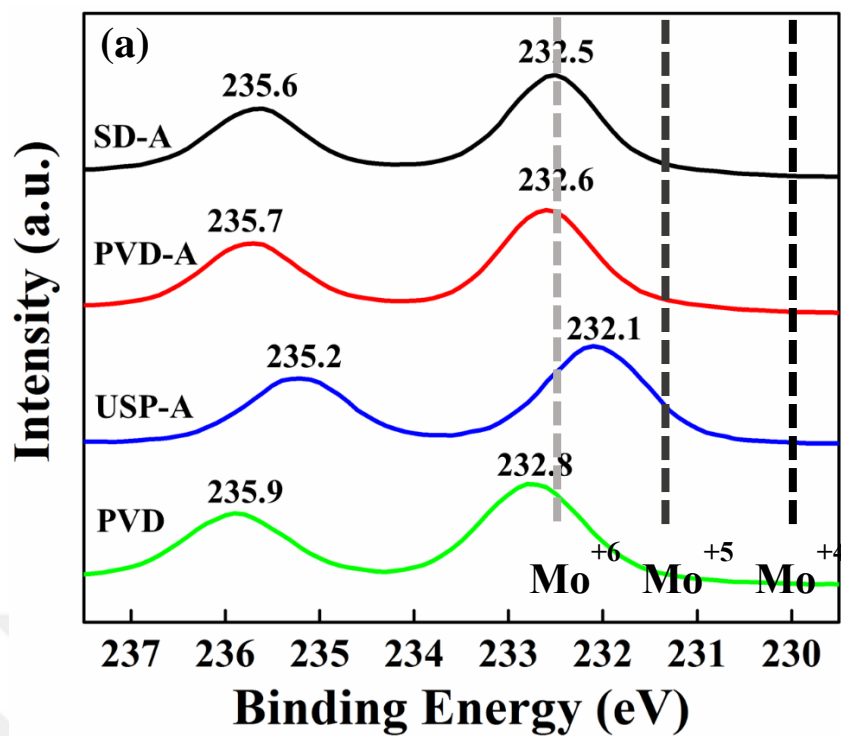


Figure 3.4 High-resolution regional XPS spectra of the samples corresponding to (a) Mo 3d 3/2 and Mo 3d 5/2 and (b) O 1s for the samples.

3.2.3. SEM Imaging

SEM images of the PVD and PVD-A samples are provided in Figures 3.5 (a) and (b), respectively. These images allowed the analysis of the effect of annealing on the thermally evaporated sample. PVD sample had a relatively homogeneous and smooth surface compared to the other samples. Upon annealing at 400°C, rod-like features were observed to grow on its surface (Figure 3.5 (b)). These features are comparable to previously synthesized MoO₃ nanorods, which was significantly denser due to a catalyst based growth [96]. They may be preferable as they increase the surface area of the deposited thin film in contact with the electrolyte during EC measurements. More active sites for intercalation could lead to an increase in the device performance. SEM image of the USP-A sample is provided in Figure 3.5 (c). A rough layer on the surface is observed with nano-sized holes. Average grain size of the sample was apparently smaller compared to the other samples. A similar rough surface was observed for thin films in a previous work, which utilized spray pyrolysis method [49]. SEM image of the USP-A sample is provided in Figure 3.5 (d). Deposition route for the SD-A sample is evident from the SEM image as similar features from both PVD and USP-A samples are observed in this figure. Although surface layer of PVD and SD-A samples were expected to be identical, similar nanorod features were absent in SD-A sample. This observation suggested that the application of SD method acted as a surface modification for the USP-A sample.

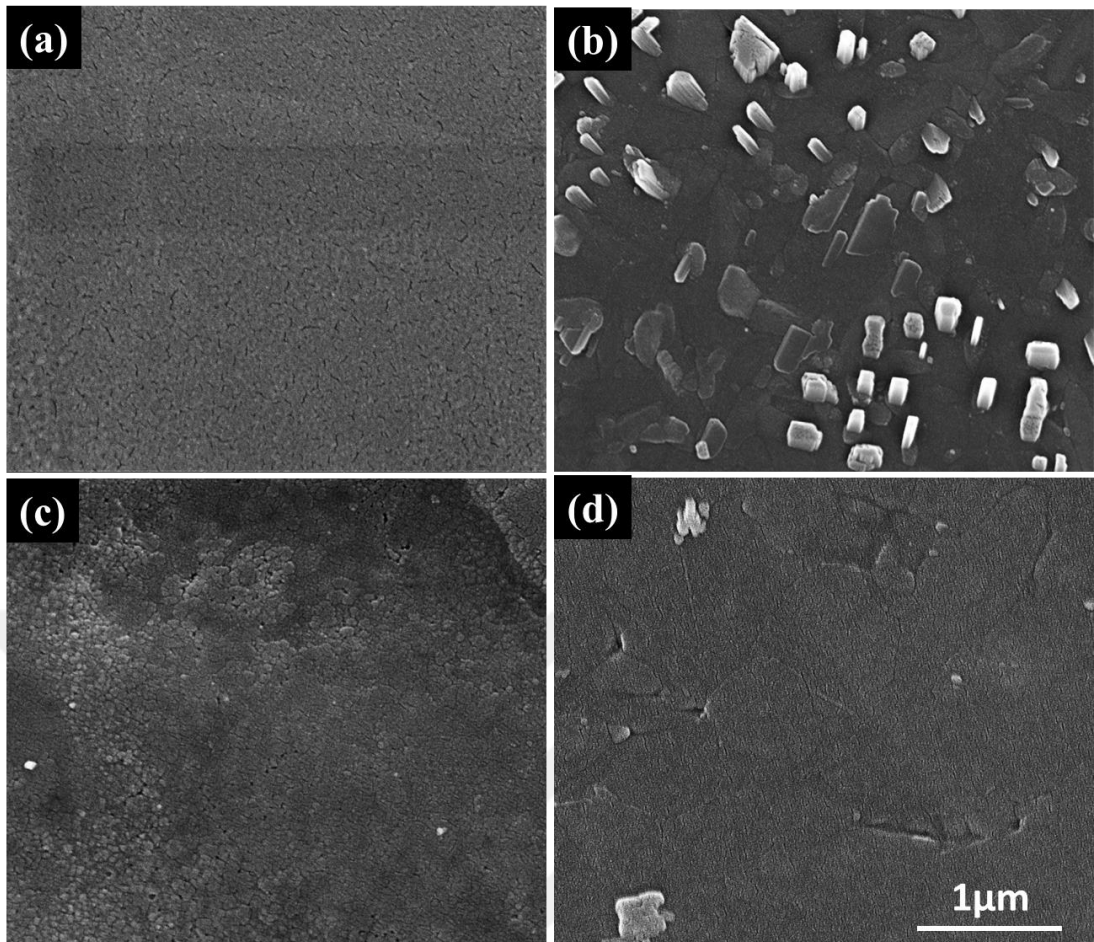


Figure 3.5 Top-view SEM images of (a) PVD, (b) PVD-A, (c) USP-A and (d) SD-A samples. All scales are the same.

3.2.4. AFM Imaging and Measurements

Topographical 3D and 2D AFM images of the USP-A sample are provided in Figures 3.6 (a) and (b), respectively. Similar to SEM images for the USP-A sample, a rough surface containing nanoparticles are evident within the AFM images. The formation mechanism of USP deposited thin film is traceable from these two images, as nanometer sized particles released from droplets by thermal effect joined together to form the thin film. In Figures 3.6 (c) and (d), AFM topographical images of PVD sample are provided. It is evident from these images that the PVD sample have a smoother surface compared to USP-A sample. Large grains on the film are predicted to occur during thermal annealing. Vertically grown nanorods observed on the

surface of the PVD-A sample are also evident in the AFM image. In Figures 3.6 (e) and (f), AFM topographical images of SD-A sample are provided. Vertically grown features were also present on this image, yet they are more widespread than those of the PVD sample. Grains of the PVD sample were clear, in contrast to those in USP-A sample, where they are tangled. For the SD-A sample, surface morphologies from both samples are present. This proves that the thermal evaporation does not completely cover and hide the features of the USP deposited thin film for SD sample.

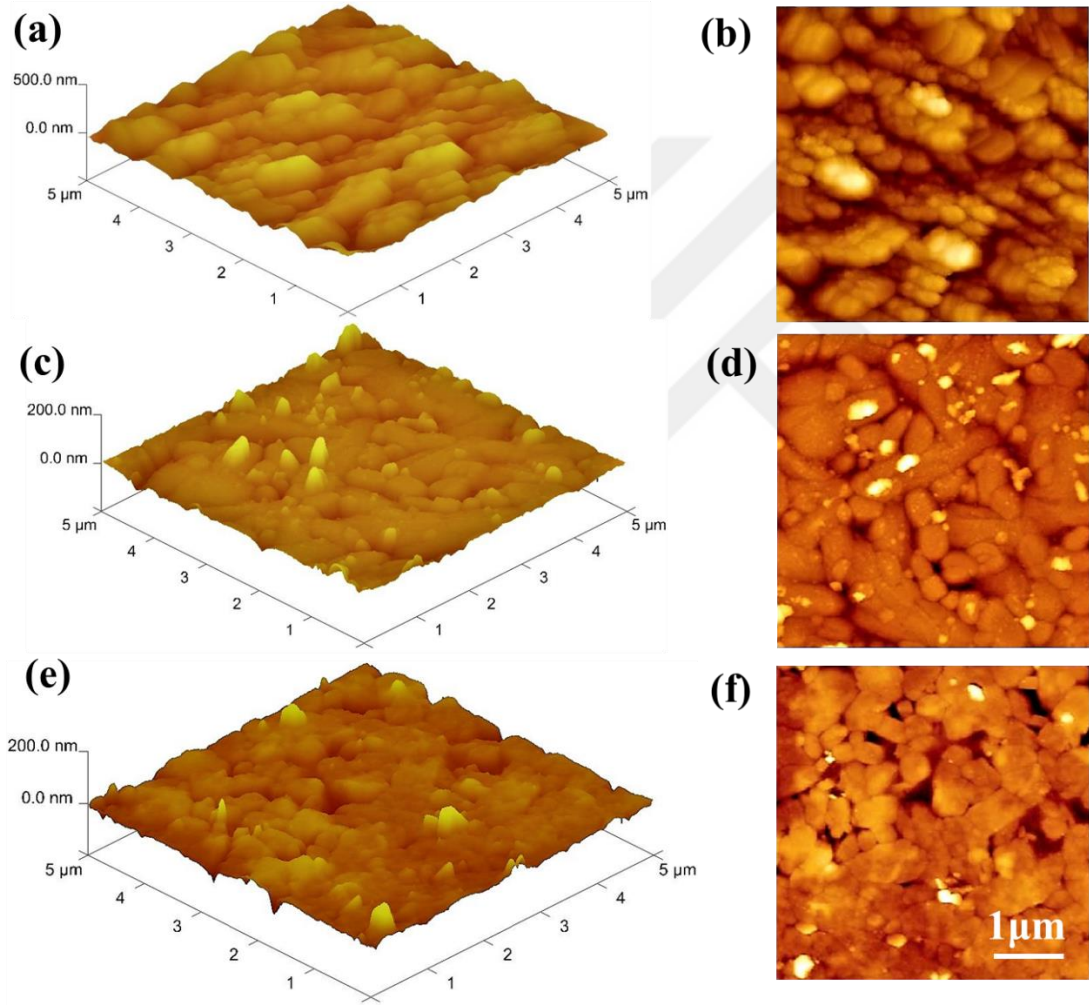


Figure 3.6 Topographical AFM 3D and 2D images of the USP-A (a,b), PVD-A (c,d) and SD-A (e,f) samples.

In Table 2, data obtained from AFM measurements were displayed. Roughness values of the films were collected from an area of 5 μm x 5 μm . RMS roughness value of the USP film (41.5 nm) was measured to be the highest among all films investigated in this work. This roughness value might be too high for solar cell applications, yet for EC layers it might be advantageous in shortening the diffusion length of ions within the electrolyte [86]. RMS roughness value of the PVD-A sample is the lowest (12.4 nm), while the RMS value of the SD-A sample (15.5 nm) is higher than that. For these two samples, high roughness was attributed to the presence of nanorod features. Average grain size measurements were also performed. Although both films were annealed at 400°C, average grain size of PVD-A was 656.5 nm, which was significantly higher than that of the USP-A sample (396 nm). Value of average grain size for the SD-A sample (535.5 nm) was placed in between that of the USP-A and PVD-A. A low grain size might be advantageous for reversibility, as grain boundaries may act as tunnels for ion transport.

Table 3.1 R_a (average roughness) and RMS (root mean square roughness) average grain size and film thickness values of each film.

	R_a (nm)	RMS (nm)	Average Grain Size (nm)	Film Thickness (nm)
USP-A	33.2	41.5	396	140
PVD-A	7.7	12.4	656.5	98.1
SD-A	10.7	15.5	535.5	182.2

3.3. EC Performance

During CV measurements, when electrode is immersed into the electrolyte solution following reactions can occur:

- 1) Cations from the electrolyte (Li^+ for this setup) can react with electroactive materials and form new phases or compounds.
- 2) Intercalation of cations into the gaps between the interlayers or van der Waals gaps (the gaps between octahedra of MoO_3) can occur. This is a reduction process and charge neutrality is maintained.
- 3) The faradaic absorption of cations onto the surface of the material.

For (2) to occur, a long range diffusion of cations through the interlayer gaps are needed. Similarly, for this process to be reversible, cations should be able to diffuse back to the electrolyte and complete the deintercalation. For both to occur sequentially, cations have to perform a long range diffusion. This is a major reason why devices operate with the mechanism of (2) tend to respond slower than devices operate with the mechanism of (3). In mechanism (3), the need for diffusion is eliminated and the intercalation occurs at the surface of the active material [97].

Cyclic voltammogram (CV) of the samples USP-A, PVD-A and SD-A are given in Figures 3.7 (a), (b) and (c), respectively. CV measurements were conducted prior to EC measurements to evaluate the electrochemical response of the MoO₃ thin films. For the evaluation, working electrode potential was switched between -2 to 2V. Samples were tested in 0.1 M LiCl₄ solutions.

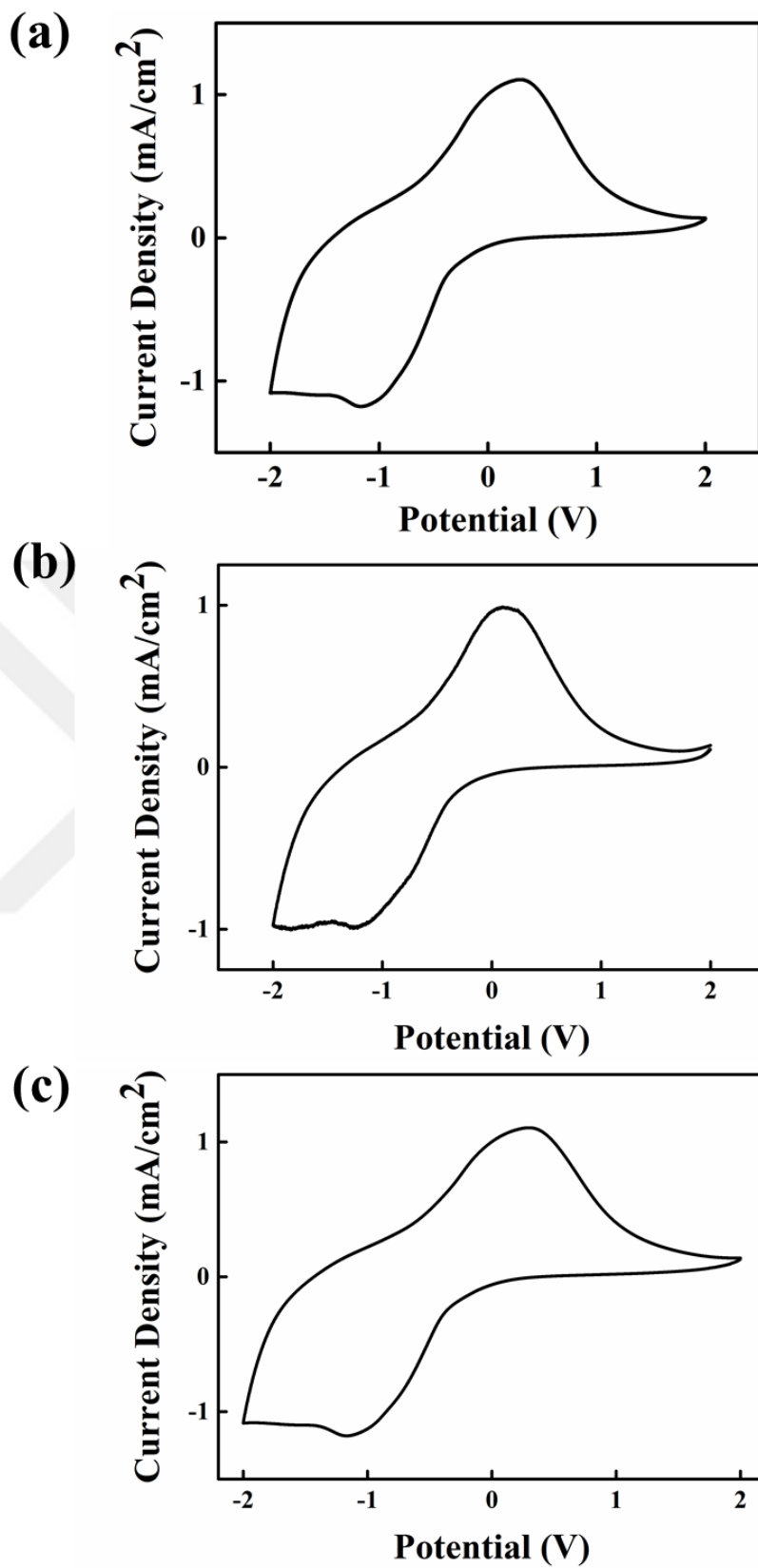


Figure 3.7 CV results of the samples (a) USP-A, (b) PVD-A and (c) SD-A.

Spectral transmittance graph of the USP-A, PVD-A and SD-A samples are provided in Figures 3.8 (a), (b) and (c), respectively. PVD sample is not reported in this part of the work since no EC response was observed. Reversible intercalation of the samples was tested through CV as the initial step. After testing the reversibility, EC response measurements were conducted. As the first data, transmittance change of USP-A sample with an applied voltage between 2 to -2 V was recorded and presented in Figure 3.8 (a). At a wavelength of 700 nm, a maximum transmittance change of 19% was observed. Similar EC transmittance change for MoO₃ thin films deposited through spray pyrolysis technique has been reported in literature [36]. A steady increase in the transmittance difference between bleached and colored states (ΔT) of USP-A sample was observed with the wavelength. Transmittance change for PVD-A sample is provided in Figures 3.8 (b). ΔT of this film within the visible spectrum was significantly higher than of that of USP, reaching 46 % at a wavelength of 570 nm. An increasing trend with an increase in wavelength was not observed for this sample unlike USP-A. In a previous research, highly crystalline and multi layered MoO₃ production was reported by thermal evaporation technique [36–38]. Thus, obtained high transmittance change is comparable and is attributed to the higher film quality of PVD-A sample compared to that of USP-A. In Figure 3.8 (c), transmittance change for SD-A sample is provided. Maximum transmittance change recorded in the visible portion of the spectrum was 27 % at a wavelength of 656 nm. Unlike USP-A and PVD-A samples, ΔT for the bleached and colored states of SD-A sample was constant within the visible spectrum.

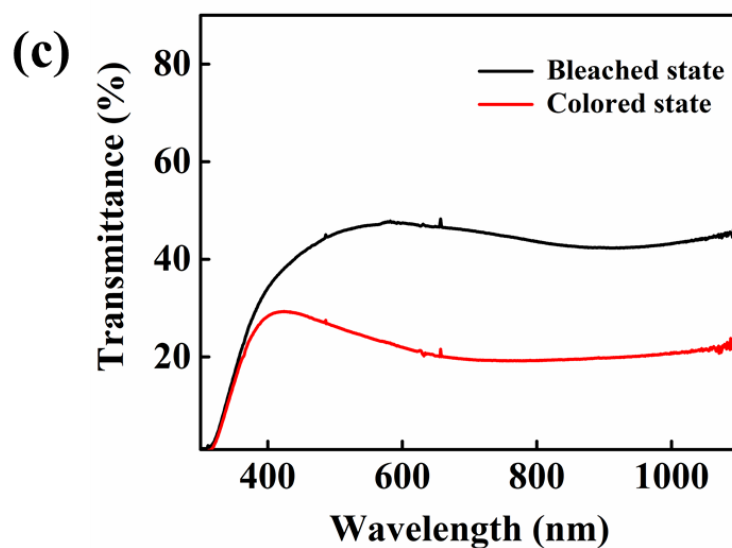
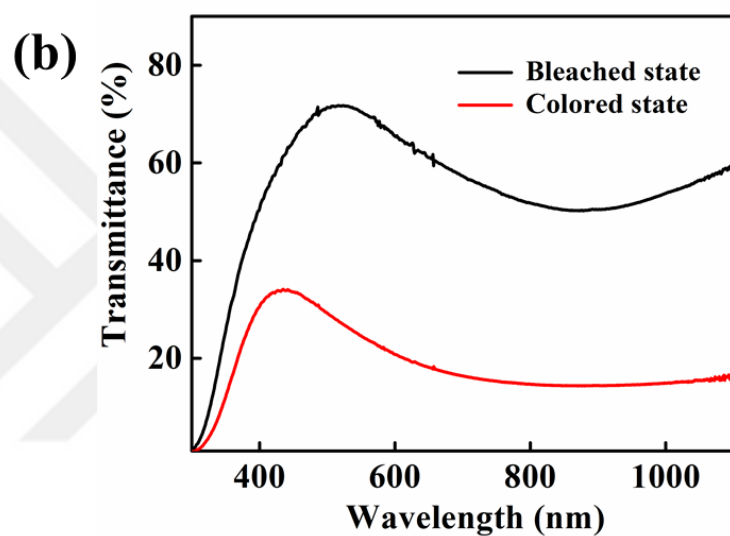
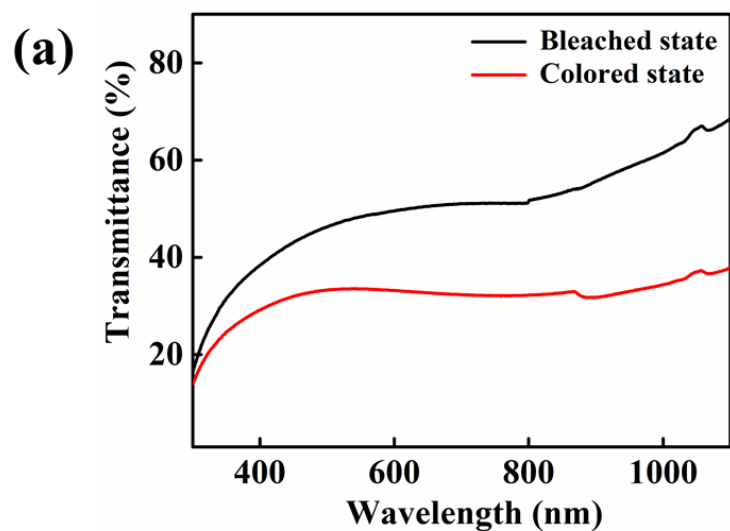


Figure 3.8 Transmittance plots for (a) USP-A, (b) PVD-A and (c) SD-A samples in bleached and colored states.

Short-term stability of the samples was evaluated by switching them between bleached and colored states at a wavelength of 700 nm. Although 700 nm was not the peak optical contrast point for some samples, comparison between the samples was performed at this point for convenience. Also 700 nm is at the boundary of the visible region, which would yield better practical information. In general, stoichiometric MoO_3 is known to have poor cycling performance when used in Li-ion battery applications [96, 97]. Since a Li based electrolyte is utilized for this work, testing of reversibility is an essential step. Evaluation of short-term stability was performed through the application of 0.01 C to all the samples in each cycle. It is important to note that transmittance changes were not the maximum values of each sample. By this method, the CE was extracted and the cyclic stability of the samples were monitored. Switching behavior of USP-A sample is shown in Figure 3.9 (a). A ΔT of 15% was obtained between the cycles for this sample. Electrode was found to be stable over the course of 4-minute cycling. In Figure 3.9 (b), cycling data for PVD-A sample is provided. Cycling is performed through the application of the same current for 4.8 seconds in each cycle. ΔT started with 21% at the first cycle, but decreased with each consecutive cycle. At the 20th cycle, ΔT was measured as 4%. Based on this data, PVD-A sample was found to be unstable under cycling. Lastly, at Figure 3.9 (c), switching behavior of SD-A sample is shown. Current with respect to time graphs of each sample is given in Figure 3.9 (d), (e), (f). Over the course of cycling, ΔT was found to be stable at 23 %. Compared to the USP-A sample, transmittance change was 7 % higher and unlike PVD-A, it was stable. In a previous work, addition of nanoparticles for the enhancement of stability of MoO_3 thin film based battery was reported [102]. Similarly, SEM and AFM images obtained from the USP-A sample investigated in this work show both nanoparticle and thin film morphology coexisting in the same structure. In addition, low average grain size value of the USP-A sample is an important contribution for the ease of ion transport and increased reversibility of the device. Thus, the high performance of SD-A sample, when compared to other samples fabricated in this work, was attributed to these parameters.

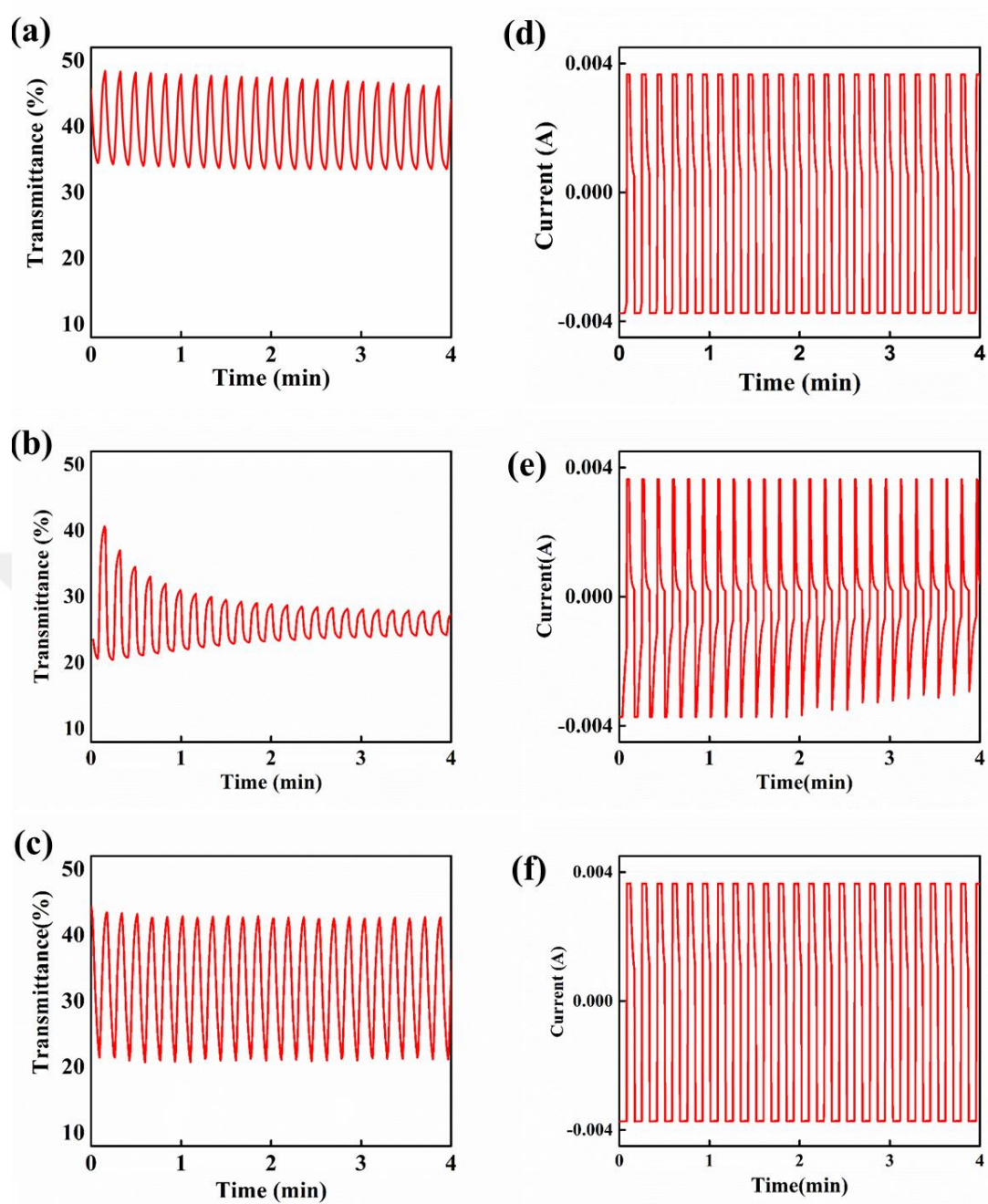


Figure 3.9 Electrochromic repeated switching and optical transmittance change and applied current with respect to time graphs of (a,d) USP-A, (b,e) PVD-A and (c,f) SD-A sample monitored at 700 nm.

EC switching time of the samples can also be evaluated from kinetic measurements. Transformation time of the samples were calculated for a ΔT of 10 % and they are given in Table 3.2. SD-A sample was observed to have the lowest switching time (1.7 sec). USP-A sample switched in 2.4 sec and PVD-A sample was the slowest with 2.9 sec.

Table 3.2 Switching time of the samples for a ΔT of 10 %.

SAMPLE	SWITCHING TIME (sec)
PVD	-
PVD-A	2.9
USP-A	2.4
SD-A	1.7

CE of the samples were calculated from ΔT , obtained by injection of 0.01 C to each sample. A high CE means easier optical modulation per inserted charge. Calculation of the optical density (OD) was simply performed according to the following formula:

$$\Delta OD = \log \left(\frac{T(\text{bleached})}{T(\text{colored})} \right) \quad (2)$$

Once the OD values for each sample was obtained, CE values were calculated using the following formula:

$$CE = \Delta OD / Q \quad (3)$$

Calculated values of the samples are tabulated and provided in Table 3.3. Calculation of CE is critical for EC applications for the purpose of evaluating their overall performance [42, 43]. Since PVD-A sample showed lower short-term coloration stability compared to other samples, calculations were carried out both for the values of initial and 20th cycle. USP-A sample maintained its CE, which was about 18 cm² C⁻¹. As obtained from Table 3.3, PVD-A sample had a CE of 30 cm² C⁻¹ at initial cycle, which decreased down to 4 cm² C⁻¹ at the 20th cycle. SD-A sample had the highest value of CE for both cycles, which is around 33 cm² C⁻¹. Results showed that,

application of SD method resulted in films with high ΔT and CE, while being stable in short-term cycling.



Table 3.3 Injected charge, transmittance values of bleached and colored states, OD and CE of the samples at the initial and 20th cycle.

	Q (C)	T (bleach %)	T (color %)	T (bleach%) 20th	T (color %) 20th	ΔOD	ΔOD 20th	CE	CE (20th)
USP-A	0.01	49	34	47	32	0.16	0.17	16	17
PVD-A	0.01	42	21	28	24	0.3	0.07	30	7
SD-A	0.01	44	21	43	20	0.32	0.33	32	33

3.4. Effect of SD Technique

EC performance of the SD sample found to be superior compared to the samples prepared by thermal evaporation and USP method. EC transformation is initiated by an externally applied voltage, which then continues with ion movement towards and away from the thin film electrochrome. Intercalation reaction executed by these ions results in an optical contrast. Characteristically, this mechanism is heavily influenced by the factors such as diffusion length of ions, reversibility of the reaction and amount of residing sites for ions. When ions are able to diffuse in and out effectively, reversibility is enhanced. Also, efficient intercalation in the structure yields high optical contrast and ΔT .

For the SD technique, deposition of MoO_3 thin film layers with both USP and thermal evaporation methods has been conducted. Characterization of the final products proved the formation of MoO_3 for all methods. Characterization with XRD and XPS methods have shown that chemical structure of the thin films fabricated by these methods are not identical. From XPS measurements, peaks at different binding energies suggested presence of different oxidation states for the samples deposited through thermal evaporation and USP methods. When these deposition methods are combined in SD method, resulting structure is expected to have a richer chemical structure due to varying oxidation states.

SEM and AFM images have shown that thin film structure deposited with USP method is porous, richer in terms of grain boundaries and presence of nanoparticles. Due to the nature of the deposition technique, some nanoparticles formed by the vaporization of solvent within the aerosol reach the substrate and initiate a porous film growth. This is visible by both monitoring techniques. This phenomenon creates a thin film with higher surface area compared to a smooth one. As it is a beneficial part of the USP technique, MoO_3 thin film formed by USP contains Mo^{+4} and Mo^{+5} states in higher concentration than the other samples. An enhanced p-type behavior is expected by this layer compared to thermal evaporated one due to higher concentration of oxygen vacancies in the structure. Overall, this yields a highly

stable structure in terms of EC performance; but, lower optical contrast due to inefficient oxidation states. This is also proved by the EC measurements taken from the thin film MoO_3 prepared by thermal evaporation. Being lowest in roughness, having highest concentration of Mo^{+6} among the other samples, it had the highest optical contrast; but, it was only reversible for a few cycles. As stated previously, chemical nature of the thin film is not the only criteria for the optimum EC performance, while efficient ion penetration, high number of residing sites for these ions and efficient ion removal after deintercalation are also compulsory.

For the application of SD, a base structure with USP method is formed. From the characterization steps, it can be stated that this base structure has high surface area, porous structure, rough surface and high density of grain boundaries. Higher concentration of Mo^{+4} and Mo^{+5} oxidation states suggests an analogy with non-stoichiometric MoO_3 layer. On top of this layer, another MoO_3 layer is deposited but through thermal evaporation this time. This layer is stoichiometric in nature and is formed by high amount of Mo^{+6} . In light of the results, it can be stated that USP base layer provides porosity, sites for ions to reside and enhances ion diffusion length. As stated before, variety of oxidation states among a metal oxide thin film in contact with an electrolyte is beneficial. This would enhance the chemical activity of the overall layer.

In summary, MoO_3 thin films deposited by SD method have beneficial characteristics over the counterparts deposited by USP and thermal evaporation methods. These characteristics were observed to contribute to the EC performance in this work. To evaluate the possibility of adaptation of SD technique to industry, opportunity cost analysis is required on the end product. Purchasing of two different thin film deposition equipments, slow deposition time of thermal evaporation due to vacuum requirement are the two disadvantages of SD method. On the contrary, possibility of fabrication of stable and high optical contrast EC devices is the advantages of this method.

CHAPTER 4

CONCLUSIONS AND FUTURE WORK

EC electrodes based on MoO₃ thin films were fabricated and their EC performance was evaluated. Application of SD through combination of thermal evaporation and USP methods are found to yield high CE, stability and high ΔT values between colored and bleached states of the EC devices. Results suggest that thermal evaporation of MoO₃ onto USP deposited MoO₃ acts as a surface modifier. It was observed that, SD method is applicable for the reduction of the surface roughness of MoO₃, providing an increase in EC performance of the thin films. The oxidation level of MoO₃ was found to depend on the deposition method used. High CE (33 cm² C⁻¹) and stability of SD deposited sample investigated in this work was highly promising and necessitate further research on SD deposition of MoO₃ and as well as other metal oxide thin films for various optoelectronic applications. As a future work, testing of the devices with CV method with longer number of cycles can be performed. Long term stability is a major problem for transition metal oxide based EC devices and addition of TiO₂ can be implemented to solve stability issues.

It is clear that spray pyrolysis method is highly suitable for the fabrication of electrochromic layers since a film roughness is highly critical in electrochrome layers. This is due to ease of ion diffusion into the thin film. Ions can travel through MoO₃ octahedra and reside there, which would similarly establish reversibility of the films.

High temperature compatibility of the transition metal oxides was also advantageous here. It enabled us to perform annealing at 400°C, pushing the crystallization and removing any contaminations caused by carbon and precursor water. With high purity and crystallization of the thin films, EC performance was enhanced. Attempts to use as deposited samples (without annealing) failed to show EC performance. In

light of this information, it can be stated that the crystallinity is highly critical for transition metal oxide electrochromes deposited by USP method.

Except WO_3 and MoO_3 , spray pyrolysis is not an ideal deposition method for transition metal oxides to be used as electrochromic layers. CE and ΔT values of other transition metal oxides, i.e. V_2O_5 , are low. Through deposition via a solution based system, these values would decrease even further. Chromic potential of the material deposited by USP should be evaluated first and it must be a considerable value for the fabrication to yield results.

Device applications of MoO_3 and WO_3 should be applied with USP method. Although solar cell and OLED charge injection layer applications demand very low roughness (1-2 nm), extensive practice of USP deposition may lead to such roughness values.

Another possible application of thin film deposition with USP system is multilayer deposition. For vacuum based methods, utilization of multilayer deposition is time consuming due to vacuum medium requirement. In contrast, deposition of separate layers on top of each is practical for the USP method. Similarly, doped structures can also be implemented easy for this method.

REFERENCES

- [1] K. Seshan, *Handbook of Thin Film Deposition*. 2012.
- [2] D. M. Mattox, *Handbook of Physical Vapor Deposition (PVD) Processing*. 1998.
- [3] P. Martin, *Ion Plating*. 2010.
- [4] H. O. Pierson, W. A. Publishing, and N. York, *Handbook of Chemical Vapor Deposition (CVD)*, no. Cvd. 1999.
- [5] R. Kaindl *et al.*, “Synthesis of Graphene-layer Nanosheet Coatings by PECVD,” in *Materials Today: Proceedings*, 2015, vol. 2, no. 8, pp. 4247–4255.
- [6] R. W. Johnson, A. Hultqvist, and S. F. Bent, “A brief review of atomic layer deposition: From fundamentals to applications,” *Mater. Today*, vol. 17, no. 5, pp. 236–246, 2014.
- [7] C. R. Kagan, “Organic-Inorganic Hybrid Materials as Semiconducting Channels in Thin-Film Field-Effect Transistors,” *Science (80-.)*, vol. 286, no. 5441, pp. 945–947, 1999.
- [8] J. M. Bian, X. M. Li, X. D. Gao, W. D. Yu, and L. D. Chen, “Deposition and electrical properties of N-In codoped p-type ZnO films by ultrasonic spray pyrolysis,” *Appl. Phys. Lett.*, vol. 84, no. 4, pp. 541–543, 2004.
- [9] A. Djelloul, M. S. Aida, and J. Bougdira, “Photoluminescence, FTIR and X-ray diffraction studies on undoped and Al-doped ZnO thin films grown on polycrystalline γ -alumina substrates by ultrasonic spray pyrolysis,” *J. Lumin.*, vol. 130, no. 11, pp. 2113–2117, 2010.
- [10] A. Duret and M. Grätzel, “Visible light-induced water oxidation on mesoscopic α -Fe₂O₃ films made by ultrasonic spray pyrolysis,” *J. Phys. Chem. B*, vol. 109, no. 36, pp. 17184–17191, 2005.
- [11] L. Castañeda, J. C. Alonso, A. Ortiz, E. Andrade, J. M. Saniger, and J. G. Bañuelos, “Spray pyrolysis deposition and characterization of titanium oxide thin films,” *Mater. Chem. Phys.*, vol. 77, pp. 938–944, 2002.
- [12] D. Perednis and L. J. Gauckler, “Thin film deposition using spray pyrolysis,” *J. Electroceramics*, vol. 14, no. 2, pp. 103–111, 2005.
- [13] S. E. Skrabalak and K. S. Suslick, “Porous MoS₂ synthesized by ultrasonic spray pyrolysis,” *J. Am. Chem. Soc.*, vol. 127, no. 28, pp. 9990–9991, 2005.
- [14] G. L. Messing, S. -C Zhang, and G. V. Jayanthi, “Ceramic Powder Synthesis

- by Spray Pyrolysis,” *J. Am. Ceram. Soc.*, vol. 76, no. 11, pp. 2707–2726, 1993.
- [15] S. D. Lee, S.-H. Nam, M.-H. Kim, and J.-H. Boo, “Synthesis and Photocatalytic Property of ZnO nanoparticles Prepared by Spray-Pyrolysis Method,” *Phys. Procedia*, vol. 32, pp. 320–326, 2012.
- [16] A. Chithambararaj and A. C. Bose, “Hydrothermal synthesis of hexagonal and orthorhombic MoO₃ nanoparticles,” *J. Alloys Compd.*, vol. 509, no. 31, pp. 8105–8110, 2011.
- [17] R. Sivakumar, R. Gopalakrishnan, M. Jayachandran, and C. Sanjeeviraja, “Characterization on electron beam evaporated α -MoO₃ thin films by the influence of substrate temperature,” *Curr. Appl. Phys.*, vol. 7, no. 1, pp. 51–59, 2007.
- [18] Y. Chen, C. Lu, L. Xu, Y. Ma, W. Hou, and J.-J. Zhu, “Single-crystalline orthorhombic molybdenum oxide nanobelts: synthesis and photocatalytic properties,” *CrystEngComm*, vol. 12, no. 11, p. 3740, 2010.
- [19] T. Mizushima, Y. Moriya, N. H. H. Phuc, H. Ohkita, and N. Kakuta, “Soft chemical transformation of α -MoO₃ to β -MoO₃ as a catalyst for vapor-phase oxidation of methanol,” *Catal. Commun.*, vol. 13, no. 1, pp. 10–13, 2011.
- [20] Z. Lei, X. Yang, J. Dong, and X. Yi, “Novel metastable hexagonal MoO₃ nanobelts: Synthesis, photochromic, and electrochromic properties,” *Chem. Mater.*, vol. 21, no. 23, pp. 5681–5690, 2009.
- [21] Y. Wang, Y. Zhu, Z. Xing, and Y. Qian, “Hydrothermal synthesis of α -MoO₃ and the influence of later heat treatment on its electrochemical properties,” *Int. J. Electrochem. Sci.*, vol. 8, no. 7, pp. 9851–9857, 2013.
- [22] J. N. Yao, B. H. Loo, K. Hashimoto, and A. Fujishima, “Photochromic and electrochromic behavior of electrodeposited molybdenum trioxide thin films,” *J. Electroanal. Chem. Interfacial Electrochem.*, vol. 290, pp. 263–267, 1990.
- [23] S. Murase and Y. Yang, “Solution processed MoO₃ interfacial layer for organic photovoltaics prepared by a facile synthesis method,” *Adv. Mater.*, vol. 24, no. 18, pp. 2459–2462, 2012.
- [24] B. Mendoza-Sánchez, T. Brousse, C. Ramirez-Castro, V. Nicolosi, and P. S. Grant, “An investigation of nanostructured thin film α -MoO₃ based supercapacitor electrodes in an aqueous electrolyte,” *Electrochim. Acta*, vol. 91, pp. 253–260, 2013.
- [25] H. Farsi, F. Gobal, H. Raissi, and S. Moghiminia, “On the pseudocapacitive behavior of nanostructured molybdenum oxide,” in *Journal of Solid State Electrochemistry*, 2010, vol. 14, no. 4, pp. 643–650.
- [26] H. Kanno, R. J. Holmes, Y. Sun, S. Kena-Cohen, and S. R. Forrest, “White stacked electrophosphorescent organic light-emitting devices employing MoO₃ as a charge-generation layer,” *Adv. Mater.*, vol. 18, no. 3, pp. 339–342,

2006.

- [27] C. Giroto, E. Voroshazi, D. Cheyns, P. Heremans, and B. P. Rand, "Solution-Processed MoO₃ Thin Films As a Hole-Injection Layer for Organic Solar Cells," *ACS Appl. Mater. Interfaces*, vol. 3, no. 9, pp. 3244–3247, 2011.
- [28] C. S. Hsu, C. C. Chan, H. T. Huang, C. H. Peng, and W. C. Hsu, "Electrochromic properties of nanocrystalline MoO₃ thin films," *Thin Solid Films*, vol. 516, no. 15, pp. 4839–4844, 2008.
- [29] T. M. McEvoy, K. J. Stevenson, J. T. Hupp, and X. Dang, "Electrochemical preparation of molybdenum trioxide thin films: Effect of sintering on electrochromic and electroinsertion properties," *Langmuir*, vol. 19, no. 10, pp. 4316–4326, 2003.
- [30] K. A. Gesheva, A. Cziraki, T. Ivanova, and A. Szekeres, "Crystallization of chemically vapor deposited molybdenum and mixed tungsten/molybdenum oxide films for electrochromic application," *Thin Solid Films*, vol. 515, no. 11, pp. 4609–4613, 2007.
- [31] T. Stubhan *et al.*, "High shunt resistance in polymer solar cells comprising a MoO₃ hole extraction layer processed from nanoparticle suspension," *Appl. Phys. Lett.*, vol. 98, no. 25, 2011.
- [32] K. Hosono, I. Matsubara, N. Murayama, S. Woosuck, and N. Izu, "Synthesis of polypyrrole/MoO₃ hybrid thin films and their volatile organic compound gas-sensing properties," *Chem. Mater.*, vol. 17, no. 2, pp. 349–354, 2005.
- [33] K. A. Gesheva and T. Ivanova, "A low-temperature atmospheric pressure CVD process for growing thin films of MoO₃ and MoO₃-WO₃ for electrochromic device applications," *Chem. Vap. Depos.*, vol. 12, no. 4, pp. 231–238, 2006.
- [34] U. O. Krašovec, A. Š. Vuk, and B. Orel, "Comparative studies of 'all sol-gel' electrochromic windows employing various counter-electrodes," *Sol. Energy Mater. Sol. Cells*, vol. 73, no. 1, pp. 21–37, 2002.
- [35] A. Agrawal, J. P. Cronin, and R. Zhang, "Review of solid state electrochromic coatings produced using sol-gel techniques," *Sol. Energy Mater. Sol. Cells*, vol. 31, no. 1, pp. 9–21, 1993.
- [36] S. S. Mahajan, S. H. Mujawar, P. S. Shinde, A. I. Inamdar, and P. S. Patil, "Concentration dependent structural, optical and electrochromic properties of MoO₃ thin films," *Int. J. Electrochem. Sci.*, vol. 3, no. 8, pp. 953–960, 2008.
- [37] A. Bouzidi, N. Benramdane, H. Tabet-Derraz, C. Mathieu, B. Khelifa, and R. Desfeux, "Effect of substrate temperature on the structural and optical properties of MoO₃ thin films prepared by spray pyrolysis technique," *Mater. Sci. Eng. B*, vol. 97, no. 1, pp. 5–8, 2003.
- [38] P. R. Patil and P. S. Patil, "Preparation of mixed oxide MoO₃-WO₃ thin films by spray pyrolysis technique and their characterization," *Thin Solid Films*, vol. 382, no. 1–2, pp. 13–22, 2001.

- [39] H. M. Martínez, J. Torres, L. D. López Carreño, and M. E. Rodríguez-García, “Effect of the substrate temperature on the physical properties of molybdenum tri-oxide thin films obtained through the spray pyrolysis technique,” *Mater. Charact.*, vol. 75, pp. 184–193, 2013.
- [40] M. Kröger, S. Hamwi, J. Meyer, T. Riedl, W. Kowalsky, and A. Kahn, “P-type doping of organic wide band gap materials by transition metal oxides: A case-study on Molybdenum trioxide,” *Org. Electron. physics, Mater. Appl.*, vol. 10, no. 5, pp. 932–938, 2009.
- [41] W.-Q. Yang, Z.-R. Wei, X.-H. Zhu, and D.-Y. Yang, “Strong influence of substrate temperature on the growth of nanocrystalline MoO₃ thin films,” *Phys. Lett. A*, vol. 373, no. 43, pp. 3965–3968, 2009.
- [42] M. B. Rahmani *et al.*, “Gas sensing properties of thermally evaporated lamellar MoO₃,” *Sensors and Actuators B-Chemical*, vol. 145, no. 1, pp. 13–19, 2010.
- [43] S. K. Deb and J. A. Chopoorian, “Optical properties and color-center formation in thin films of molybdenum trioxide,” *J. Appl. Phys.*, vol. 37, no. 13, pp. 4818–4825, 1966.
- [44] M. Diskus, O. Nilsen, and H. Fjellvåg, “Growth of thin films of molybdenum oxide by atomic layer deposition,” *J. Mater. Chem.*, vol. 21, no. 3, p. 705, 2011.
- [45] M. Ferroni, V. Guidi, G. Martinelli, P. Nelli, M. Sacerdoti, and G. Sberveglieri, “Characterization of a molybdenum oxide sputtered thin film as a gas sensor,” *Thin Solid Films*, vol. 307, no. 1–2, pp. 148–151, 1997.
- [46] D. Mutschall, K. Holzner, and E. Obermeier, “Sputtered molybdenum oxide thin films for NH₃ detection,” *Sensors and Actuators B-Chemical*, vol. 36, no. 1–3, pp. 320–324, 1996.
- [47] C. Imawan, H. Steffes, F. Solzbacher, and E. Obermeier, “A new preparation method for sputtered MoO₃ multilayers for the application in gas sensors,” *Sensors Actuators, B Chem.*, vol. 78, no. 1–3, pp. 119–125, 2001.
- [48] M. Dhanasankar, K. K. Purushothaman, and G. Muralidharan, “Effect of temperature of annealing on optical, structural and electrochromic properties of sol-gel dip coated molybdenum oxide films,” *Appl. Surf. Sci.*, vol. 257, pp. 2074–2079, 2011.
- [49] D. Di Yao, J. Z. Ou, K. Latham, S. Zhuiykov, A. P. O’Mullane, and K. Kalantar-Zadeh, “Electrodeposited ??- And ??-phase MoO₃ films and investigation of their gasochromic properties,” *Cryst. Growth Des.*, vol. 12, no. 4, pp. 1865–1870, 2012.
- [50] J. Meyer, R. Khalandovsky, P. Görrn, and A. Kahn, “MoO₃ films spin-coated from a nanoparticle suspension for efficient hole-injection in organic electronics,” *Adv. Mater.*, vol. 23, no. 1, pp. 70–73, 2011.
- [51] R. J. Mortimer, D. R. Rosseinsky, and P. M. S. Monk, *Electrochromic*

- [52] K. Liang, D. B. Mitzi, and M. T. Prikas, "Synthesis and Characterization of Organic–Inorganic Perovskite Thin Films Prepared Using a Versatile Two-Step Dipping Technique," *Chem. Mater.*, vol. 10, no. 1, pp. 403–411, 1998.
- [53] D. Bi *et al.*, "Using a two-step deposition technique to prepare perovskite (CH₃NH₃PbI₃) for thin film solar cells based on ZrO₂ and TiO₂ mesostructures," *RSC Adv.*, vol. 3, no. 41, p. 18762, 2013.
- [54] J. Burschka *et al.*, "Sequential deposition as a route to high-performance perovskite-sensitized solar cells.," *Nature*, vol. 499, no. 7458, pp. 316–320, 2013.
- [55] C. G. Granqvist, "Electrochromic tungsten oxide films: Review of progress 1993-1998," *Sol. Energy Mater. Sol. Cells*, vol. 60, no. 3, pp. 201–262, 2000.
- [56] S. H. Baeck, K. S. Choi, T. F. Jaramillo, G. D. Stucky, and E. W. McFarland, "Enhancement of photocatalytic and electrochromic properties of electrochemically fabricated mesoporous WO₃ thin films," *Adv. Mater.*, vol. 15, no. 15, pp. 1269–1273, 2003.
- [57] S. H. Lee *et al.*, "Crystalline WO₃ nanoparticles for highly improved electrochromic applications," *Adv. Mater.*, vol. 18, no. 6, pp. 763–766, 2006.
- [58] R. D. Rauh, F. Wang, J. R. Reynolds, and D. L. Meeker, "High coloration efficiency electrochromics and their application to multi-color devices," *Electrochim. Acta*, vol. 46, no. 13–14, pp. 2023–2029, 2001.
- [59] Y. C. Nah, A. Ghicov, D. Kim, and P. Schmuki, "Enhanced electrochromic properties of self-organized nanoporous WO₃," *Electrochem. commun.*, vol. 10, no. 11, pp. 1777–1780, 2008.
- [60] A. Cremonesi, D. Bersani, P. P. Lottici, Y. Djaoued, and P. V. Ashrit, "WO₃ thin films by sol-gel for electrochromic applications," in *Journal of Non-Crystalline Solids*, 2004, vol. 345–346, pp. 500–504.
- [61] J. M. O. R. De León, D. R. Acosta, U. Pal, and L. Castañeda, "Improving electrochromic behavior of spray pyrolysed WO₃ thin solid films by Mo doping," *Electrochim. Acta*, vol. 56, no. 5, pp. 2599–2605, 2011.
- [62] E. Pehlivan, F. Z. Tepehan, and G. G. Tepehan, "Comparison of optical, structural and electrochromic properties of undoped and WO₃-doped Nb₂O₅ thin films," in *Solid State Ionics*, 2003, vol. 165, no. 1–4, pp. 105–110.
- [63] L. Liang *et al.*, "High-performance flexible electrochromic device based on facile semiconductor-to-metal transition realized by WO₃·2H₂O ultrathin nanosheets.," *Sci. Rep.*, vol. 3, p. 1936, 2013.
- [64] H. Zheng, Y. Tachibana, and K. Kalantar-Zadeh, "Dye-sensitized solar cells based on WO₃," *Langmuir*, vol. 26, no. 24, pp. 19148–19152, 2010.
- [65] A. Gheno, T. T. Thu Pham, C. Di Bin, J. Boucl??, B. Ratier, and S. Vedraïne, "Printable WO₃ electron transporting layer for perovskite solar cells:

- Influence on device performance and stability,” *Sol. Energy Mater. Sol. Cells*, vol. 161, pp. 347–354, 2017.
- [66] K. Mahmood, B. S. Swain, A. R. Kirmani, and A. Amassian, “Highly efficient perovskite solar cells based on a nanostructured WO₃-TiO₂ core-shell electron transporting material,” *J. Mater. Chem. A*, vol. 3, no. 17, pp. 9051–9057, 2015.
- [67] K. Galatsis, Y. X. Li, W. Wlodarski, and K. Kalantar-zadeh, “Sol-gel prepared MoO₃-WO₃ thin-films for O₂ gas sensing,” *Sensors Actuators, B Chem.*, vol. 77, no. 1–2, pp. 478–483, 2001.
- [68] B. O’Regan and M. Grätzel, “A low-cost, high-efficiency solar cell based on dye-sensitized colloidal TiO₂ films,” *Nature*, vol. 353, no. 6346, pp. 737–740, 1991.
- [69] U. Opara Krašovec, M. Berginc, M. Hočevar, and M. Topič, “Unique TiO₂ paste for high efficiency dye-sensitized solar cells,” *Sol. Energy Mater. Sol. Cells*, vol. 93, no. 3, pp. 379–381, 2009.
- [70] J. Wang and Z. Lin, “Dye-sensitized TiO₂ nanotube solar cells with markedly enhanced performance via rational surface engineering,” *Chem. Mater.*, vol. 22, no. 2, pp. 579–584, 2010.
- [71] S. M. Gupta and M. Tripathi, “A review of TiO₂ nanoparticles,” *Chinese Science Bulletin*, vol. 56, no. 16, pp. 1639–1657, 2011.
- [72] S. K. Choi, S. Kim, S. K. Lim, and H. Park, “Photocatalytic comparison of TiO₂ nanoparticles and electrospun TiO₂ nanofibers: Effects of mesoporosity and interparticle charge transfer,” *J. Phys. Chem. C*, vol. 114, no. 39, pp. 16475–16480, 2010.
- [73] A. Benoit, I. Paramasivam, Y. C. Nah, P. Roy, and P. Schmuki, “Decoration of TiO₂ nanotube layers with WO₃ nanocrystals for high-electrochromic activity,” *Electrochem. commun.*, vol. 11, no. 4, pp. 728–732, 2009.
- [74] C. M. Wang and S. Y. Lin, “Electrochromic properties of sputtered TiO₂ thin films,” *J. Solid State Electrochem.*, vol. 10, no. 4, pp. 255–259, 2006.
- [75] T. Ivanova, A. Harizanova, T. Koutzarova, N. Krins, and B. Vertruyen, “Electrochromic TiO₂, ZrO₂ and TiO₂-ZrO₂ thin films by dip-coating method,” *Mater. Sci. Eng. B Solid-State Mater. Adv. Technol.*, vol. 165, no. 3, pp. 212–216, 2009.
- [76] H. K. Jheong, Y. J. Kim, J. H. Pan, T. Y. Won, and W. I. Lee, “Electrochromic property of the viologen-anchored mesoporous TiO₂ films,” in *Journal of Electroceramics*, 2006, vol. 17, no. 2–4, pp. 929–932.
- [77] A. A. Argun *et al.*, “Multicolored electrochromism in polymers: Structures and devices,” *Chemistry of Materials*, vol. 16, no. 23, pp. 4401–4412, 2004.
- [78] A. Jonsson and A. Roos, “Evaluation of control strategies for different smart window combinations using computer simulations,” *Sol. Energy*, vol. 84, no. 1, pp. 1–9, 2010.

- [79] P. M. S. Monk, F. Delage, and S. M. Costa Vieira, "Electrochromic paper: Utility of electrochromes incorporated in paper," *Electrochim. Acta*, vol. 46, no. 13–14, pp. 2195–2202, 2001.
- [80] C.-P. Li, F. Lin, R. M. Richards, C. Engtrakul, R. C. Tenent, and C. a. Wolden, "The influence of sol–gel processing on the electrochromic properties of mesoporous WO₃ films produced by ultrasonic spray deposition," *Sol. Energy Mater. Sol. Cells*, vol. 121, no. February, pp. 163–170, 2014.
- [81] T. Brezesinski, D. F. Rohlfiing, S. Sallard, M. Antonietti, and B. M. Smarsly, "Highly crystalline WO₃ thin films with ordered 3D mesoporosity and improved electrochromic performance," *Small*, vol. 2, no. 10, pp. 1203–1211, 2006.
- [82] B. W. Faughnan and R. S. Crandall, "Optical properties of mixed-oxide WO₃/MoO₃ electrochromic films," *Appl. Phys. Lett.*, vol. 31, no. 12, pp. 834–836, 1977.
- [83] P. M. S. Monk, R. J. Mortimer, and D. R. Rosseinsky, *Electrochromism and electrochromic devices*, no. 1. 2007.
- [84] D. T. Gillaspie, R. C. Tenent, and A. C. Dillon, "Metal-oxide films for electrochromic applications: present technology and future directions," *J. Mater. Chem.*, vol. 20, no. 43, p. 9585, 2010.
- [85] H.-C. Chen, D.-J. Jan, C.-H. Chen, and K.-T. Huang, "Bond and electrochromic properties of WO₃ films deposited with horizontal DC, pulsed DC, and RF sputtering," *Electrochim. Acta*, vol. 93, pp. 307–313, 2013.
- [86] C. G. Granqvist, *Handbook of Inorganic Electrochromic Materials*. 1995.
- [87] R. S. Patil, M. D. Uplane, and P. S. Patil, "Electrosynthesis of electrochromic molybdenum oxide thin films with rod-like features," *Int. J. Electrochem. Sci.*, vol. 3, no. 3, pp. 259–265, 2008.
- [88] D. D. Yao, R. A. Rani, A. P. O'Mullane, K. Kalantar-zadeh, and J. Z. Ou, "Enhanced Coloration Efficiency for Electrochromic Devices based on Anodized Nb₂O₅/Electrodeposited MoO₃ Binary Systems," *J. Phys. Chem. C*, vol. 118, no. 20, pp. 10867–10873, 2014.
- [89] N. K. Shrestha, Y.-C. Nah, H. Tsuchiya, and P. Schmuki, "Self-organized nano-tubes of TiO₂–MoO₃ with enhanced electrochromic properties," *Chem. Commun.*, no. 15, p. 2008, 2009.
- [90] D. Di Yao, M. R. Field, A. P. O'Mullane, K. Kalantar-zadeh, and J. Z. Ou, "Electrochromic properties of TiO₂ nanotubes coated with electrodeposited MoO₃," *Nanoscale*, vol. 5, no. 21, p. 10353, 2013.
- [91] J. Światowska-Mrowiecka *et al.*, "Li-ion intercalation in thermal oxide thin films of MoO₃ as studied by XPS, RBS, and NRA," *J. Phys. Chem. C*, vol. 112, no. 29, pp. 11050–11058, 2008.
- [92] Y. Zhu *et al.*, "A cost-effective commercial soluble oxide cluster for highly

- efficient and stable organic solar cells,” *J. Mater. Chem. A*, vol. 2, no. 5, pp. 1436–1442, 2014.
- [93] M. T. Greiner, L. Chai, M. G. Helander, W. M. Tang, and Z. H. Lu, “Metal/metal-oxide interfaces: How metal contacts affect the work function and band structure of MoO₃,” *Adv. Funct. Mater.*, vol. 23, no. 2, pp. 215–226, 2013.
- [94] D. Briggs and J. T. Grant, “Surface Analysis by Auger and X-Ray Photoelectron Spectroscopy,” in *Surface Analysis by Auger and X-Ray Photoelectron Spectroscopy*, 2003, pp. 31–56.
- [95] D. O. Scanlon, G. W. Watson, D. J. Payne, G. R. Atkinson, R. G. Egdell, and D. S. L. Law, “Theoretical and Experimental Study of the Electronic Structures of MoO₃ and MoO₂,” *J. Phys. Chem. C*, vol. 114, no. 10, pp. 4636–4645, 2010.
- [96] L. Zheng, Y. Xu, D. Jin, and Y. Xie, “Well-aligned molybdenum oxide nanorods on metal substrates: solution-based synthesis and their electrochemical capacitor application,” *J. Mater. Chem.*, vol. 20, no. 34, p. 7135, 2010.
- [97] T. Brezesinski, J. Wang, S. H. Tolbert, and B. Dunn, “Ordered mesoporous α -MoO₃ with iso-oriented nanocrystalline walls for thin-film pseudocapacitors,” *Nat. Mater.*, vol. 9, no. 2, pp. 146–151, 2010.
- [98] J. Z. Ou, J. L. Campbell, D. Yao, W. Wlodarski, and K. Kalantar-Zadeh, “In situ Raman spectroscopy of H₂ gas interaction with layered MoO₃,” *J. Phys. Chem. C*, vol. 115, no. 21, pp. 10757–10763, 2011.
- [99] J. Yu, S. J. Ippolito, M. Shafiei, D. Dhawan, W. Wlodarski, and K. Kalantar-Zadeh, “Reverse biased Pt/nanostructured MoO₃/SiC Schottky diode based hydrogen gas sensors,” *Appl. Phys. Lett.*, vol. 94, no. 1, 2009.
- [100] J. O. Besenhard, J. Heydecke, and H. P. Fritz, “Characteristics of molybdenum oxide and chromium oxide cathodes in primary and secondary organic electrolyte lithium batteries I. Morphology, structure and their changes during discharge and cycling,” *Solid State Ionics*, vol. 6, no. 3, pp. 215–224, 1982.
- [101] M. E. Spahr, P. Novák, O. Haas, and R. Nesper, “Electrochemical insertion of lithium, sodium, and magnesium in molybdenum(VI) oxide,” *J. Power Sources*, vol. 54, no. 2, pp. 346–351, 1995.
- [102] S. H. Lee *et al.*, “Reversible lithium-ion insertion in molybdenum oxide nanoparticles,” *Adv. Mater.*, vol. 20, no. 19, pp. 3627–3632, 2008.
- [103] R. J. Mortimer Permanent address: Department and J. R. Reynolds, “In situ colorimetric and composite coloration efficiency measurements for electrochromic Prussian blue,” *J. Mater. Chem.*, vol. 15, no. 22, p. 2226, 2005.

CURRICULUM VITAE

ONUR TÜREL

Metallurgical and Materials Engineering Department,
Middle East Technical University (METU)
06800, Ankara, TURKEY.
e-mail: onurturel06@gmail.com
mobile: +90 (535) 364 0724

FORMAL EDUCATION

- *Master of Science (Candidate)*, Metallurgical and Materials Engineering Department Middle East Technical University, (METU); Ankara TURKEY
- *Bachelor of Science*, Metallurgical and Materials Engineering Department; (January 2014) Middle East Technical University (METU); Ankara TURKEY

WORK EXPERIENCE

- Galvanizing Engineer (May 2017- ongoing)
Mitas Galvanizing Inc. Ankara TURKEY

PUBLICATIONS

1. **O. Turel**, S. Hacıoğlu, S. Coşkun, L. Toppare and H. Unalan, Sequential Deposition of Electrochromic MoO₃ Thin Films with High Coloration Efficiency and Stability. (Submitted to Journal of the Electrochemical Society)
2. T. Gokoglan, S. Soylemez, M. Kesik, I. Dogru, **O. Turel**, R. Yuksel, H. Unalan, L. Toppare, A Novel Approach for the Fabrication of a Flexible Glucose Biosensor: The Combination of Vertically Aligned CNTs and a Conjugated Polymer. Food Chemistry, (2017) 220: 299–305
3. I.B. Dogru, M. B. Durukan, **O. Turel**, H.E. Unalan, Flexible supercapacitor electrodes with vertically aligned carbon nanotubes grown on aluminum foils, Prog. Nat. Sci.: Mat. Int. 26 (2016) 232-236